Journal of Autoimmunity 147 (2024) 103267

Contents lists available at ScienceDirect

Journal of Autoimmunity

journal homepage: www.elsevier.com/locate/jautimm

Diverse immunological dysregulation, chronic inflammation, and impaired erythropoiesis in long COVID patients with chronic fatigue syndrome

Suguru Saito [a,1], Shima Shahbaz [a,1], Mohammed Osman [b], Desiree Redmond [b], Najmeh Bozorgmehr [a], Rhonda J. Rosychuk [c], Grace Lam [d], Wendy Sligl [e,f], Jan Willem Cohen Tervaert [b], Shokrollah Elahi [a,g,h,i,*]

[a] School of Dentistry, Division of Foundational Sciences, Faculty of Medicine & Dentistry, University of Alberta, Edmonton, T6G 2E1, AB, Canada
[b] Department of Medicine, Division of Rheumatology, Faculty of Medicine & Dentistry, University of Alberta, Edmonton, T6G 2E1, AB, Canada
[c] Department of Pediatrics, Division of Infectious Disease, Faculty of Medicine & Dentistry, University of Alberta, Edmonton, T6G 2E1, AB, Canada
[d] Department of Medicine, Division of Pulmonary Medicine, Faculty of Medicine & Dentistry, University of Alberta, Edmonton, T6G 2E1, AB, Canada
[e] Department of Critical Care Medicine, Faculty of Medicine & Dentistry, University of Alberta, Edmonton, T6G 2E1, AB, Canada
[f] Department of Medicine, Division of Infectious Diseases, Faculty of Medicine & Dentistry, University of Alberta, Edmonton, T6G 2E1, AB, Canada
[g] Department of Oncology, University of Alberta, Edmonton, T6G 2E1, AB, Canada
[h] Faculty of Medicine & Dentistry, University of Alberta, Edmonton, T6G 2E1, AB, Canada
[i] Li Ka Shing Institute of Virology, Faculty of Medicine & Dentistry, University of Alberta, Edmonton, T6G 2E1, AB, Canada

ARTICLE INFO

Handling Editor: Professor C Selmi

Keywords:
T cell exhaustion
Inflammation and long COVID
Autoimmunity
Artemin
Galectin-9
CD71$^+$ erythroid cells
MAIT cells

ABSTRACT

A substantial number of patients recovering from acute SARS-CoV-2 infection present serious lingering symptoms, often referred to as long COVID (LC). However, a subset of these patients exhibits the most debilitating symptoms characterized by ongoing myalgic encephalomyelitis or chronic fatigue syndrome (ME/CFS). We specifically identified and studied ME/CFS patients from two independent LC cohorts, at least 12 months post the onset of acute disease, and compared them to the recovered group (R). ME/CFS patients had relatively increased neutrophils and monocytes but reduced lymphocytes. Selective T cell exhaustion with reduced naïve but increased terminal effector T cells was observed in these patients. LC was associated with elevated levels of plasma pro-inflammatory cytokines, chemokines, Galectin-9 (Gal-9), and artemin (ARTN). A defined threshold of Gal-9 and ARTN concentrations had a strong association with LC. The expansion of immunosuppressive CD71$^+$ erythroid cells (CECs) was noted. These cells may modulate the immune response and contribute to increased ARTN concentration, which correlated with pain and cognitive impairment. Serology revealed an elevation in a variety of autoantibodies in LC. Intriguingly, we found that the frequency of 2B4$^+$CD160$^+$ and TIM3$^+$CD160$^+$ CD8$^+$ T cells completely separated LC patients from the R group. Our further analyses using a multiple regression model revealed that the elevated frequency/levels of CD4 terminal effector, ARTN, CEC, Gal-9, CD8 terminal effector, and MCP1 but lower frequency/levels of TGF-β and MAIT cells can distinguish LC from the R group. Our findings provide a new paradigm in the pathogenesis of ME/CFS to identify strategies for its prevention and treatment.

1. Introduction

A portion of patients recovering from COVID-19 disease has reported a wide range of symptoms that last for many months after the onset of acute infection [1,2]. This condition is termed long COVID (LC) or post-acute COVID-19 syndrome (PACS) [3–5]. LC is composed of heterogeneous sequelae that often affect multiple organ systems and occurs in >10 % of infected people with SARS-CoV-2 [6]. Some studies suggested a role for immune alteration [7], autoantibodies [8], endothelial dysfunction [9], persistent SARS-CoV-2 tissue reservoirs [10], elevated plasma cytokines [11], and activated innate immune cells as contributors to LC [7]. Moreover, in LC patients, there is evidence of

* Corresponding author. School of Dentistry, Division of Foundational Sciences, Faculty of Medicine & Dentistry, University of Alberta, Edmonton, T6G 2E1, AB, Canada.
E-mail address: elahi@ualberta.ca (S. Elahi).
[1] Authors equally contributed.

https://doi.org/10.1016/j.jaut.2024.103267
Received 30 October 2023; Received in revised form 16 May 2024; Accepted 22 May 2024
Available online 25 May 2024

impaired energy metabolism, mitochondrial dysfunction, and notable metabolomic alterations [12,13]. Therefore, potentially multiple and likely overlapping factors are associated with LC. As an exploratory study to evaluate and identify immunological paraments associated with LC, we conducted our studies in two independent cohorts of LC patients, which developed myalgic encephalomyelitis or chronic fatigue syndrome (ME/CFS)-like symptoms one year apart. We conducted a comprehensive comparison between LC patients and age-sex-matched individuals who recovered from SARS-CoV-2 to identify the biological signature associated with LC with ME/CFS. This addresses a clinical gap in the LC field with implications extending beyond LC.

2. Material and methods

2.1. Study population

A total of 199 human subjects were recruited for both cohorts. The first cohort comprised 131 study subjects including **1**) 33 healthy controls (HCs, median age 49 ± 15.6, 24 females and 9 males); **2**) 44 LC patients (median age 51.5 ± 13.1, 33 females and 11 males); **3**) 24 COVID-19 patients who had recovered (R) from the disease without any obvious symptoms and complications per se (median age 50.5 ± 13.3, 18 females and 6 males). **4**) 30 acute COVID-19 patients (median age 66.13 ± 11.86); All individuals except HCs were infected with the original SARS-CoV-2 (Wuhan) viral strain in 2020, which was confirmed by PCR at the University of Alberta Hospital, Edmonton. Acute COVID-19 patients were recruited from those infected with the Wuhan strain and presented with mild/moderate or severe disease in 2020, as we have reported elsewhere [14]. We identified and recruited those 13 individuals from this cohort who later developed LC. Moreover, we were able to recruit 17 R individuals from the same acute COVID-19 cohort. HCs were recruited before the COVID-19 pandemic (2017–2018), and their PBMCs and plasma samples were stored frozen for later use. Both LC and R related to the first cohort were recruited ~12 months (371 ± 19 days LC vs. 368 ± 6.2 days R) after the onset of SARS-CoV-2 infection (Supplementary Table S1, Fig. 1A–C). Of note, patients in this cohort were recruited through the LC clinic at the University of Alberta Hospital, Edmonton. Similarly, age-sex-matched R participants were recruited in the same clinic from previously infected individuals with the Wuhan strain of SARS-CoV-2.

The second cohort consisted of 34 LC patients with ME/CFS (median age 48 ± 9.8, 25 females and 9 males) and 34 patients recovered (median age 45 ± 11.39, 24 females and 10 males) from SARS-CoV-2 infection without any long-term symptoms per se (Supplementary Table S2, Fig. 1A and B). Our ME/CFS patients were selected from a pool of over 2000 patients exhibiting LC symptoms. Through a comprehensive evaluation process that involved clinical assessments, laboratory tests, and the administration of well-defined questionnaires. Specifically, we utilized the de Paul Symptom Questionnaire (PSQ) to identify which patients fulfilled the criteria of ME/CFS; then used the FACIT Fatigue (Version 4) and multidimensional fatigue inventory to identify the severity of fatigue as outlined in the Canadian Consensus criteria (CDC) for ME/CFS and WHO [15,16] as we have previously described [17,18]. It is important to note that the majority of the >2000 LC patients did not present with ME/CFS, but rather exhibited other LC-related symptoms. We diligently selected those with ME/CFS from this cohort of LC patients. Similar to cohort 1, the infection was confirmed by PCR and the proof of infection with SARS-CoV-2 was obtained from the review of medical records of study subjects. This cohort was infected mainly with the Delta/or Omicron variants and a few with the original strain. In the second cohort, both LC and R groups were recruited ~12 months (435 ± 89 days LC vs. 415 ± 40 days R) after the onset of acute disease to be consistent with our first cohort (Supplementary Table S2, Fig. 1D). The second cohort was established using the help of the province of Alberta LC Facebook community and recruited at the Key Edmonton LC Clinic. The LC patients from both cohorts were precisely characterized through extensive questionnaires/clinical evaluation according to the criteria established/described for ME/CFS. As an added control group, age-sex-matched R participants were recruited in the same clinic from previously infected and recovered individuals without any clinical symptoms per se with the help of the province of Alberta Facebook community, through advertisements online, and in public places.

Study participants were age-and sex-matched and considering that the majority of our patients had a mild acute infection, confounding health conditions were not common (Supplementary Tables S1 and 2, Fig. 1B). Only a small number of LC in our first cohort (4/44, 9 %) had a history of ICU admission due to COVID-19 disease (Fig. 1B). To clarify sample distribution, these 4 patients were colored in green in figures. Similarly, in the second cohort (2/34, 5.9 %) had a history of ICU admission due to COVID-19 disease (Supplementary Table S2). Comorbidities were 15.9 % in LC and 16.6 % in R of the first cohort and 8.8 % in LC and 5.8 % in R of the second cohort. All study subjects (LC and R) in the first cohort were SAS-CoV-2 vaccine-naïve, but 67.3 % of LC and 73.5 % of R were vaccinated in the second cohort (Supplementary Tables S1 and 2). It is worth mentioning that 82.3 % and 76.4 % of our LC patients and R individuals were infected with SARS-CoV-2 prior to getting vaccinated against this virus, respectively.

We utilized a set of well-defined validated and comprehensive clinical questionnaires developed by CDC and WHO [15,16] in our clinical evaluation to capture the severity of symptoms in the LC cohorts. This was performed through in-person meetings at the time of recruitment to the study and serial clinical assessments using 7 different questionnaires including **1**) De Paul Symptom Questionnaires (DSQ) where patients were required to have at least 5/6 (with post-exertional malaise related symptoms as a criterion) for confirmation of ME/CFS [19], **2**) Functional Assessment of Chronic Illness Therapy (FACIT) Fatigue scale questionnaire; **3**) FACIT-Dyspnea; **4**) Fibromyalgia (FM) diagnostic criteria; **5**) Cognitive Failure Questionnaire (CFQ); **6**) The Pittsburgh Sleep Quality Index (PSQI): **7**) The Hospital Anxiety and Depression Scale (HADS). These questionnaires contain different items and quantifies the severity and frequency of patients' symptoms.

All participants were evaluated for the presence of criteria related to ME/CFS based on the DSQ; namely: fatigue (I), post-exertional malaise (II), sleep difficulties (III), pain (IV), neurological/cognitive manifestations (V), and other (VI) which included autonomic, neuroendocrine, and immune manifestations using a 5-point Likert scale ranging from 0: none of the time, 1: a little of the time, 2: about half the time, 3: most of the time, and 4: all of the time. The severity of the symptoms was also recorded using a 5-point Likert scale with 0: no symptom, 1: mild, 2: moderate, 3: severe, and 4: very severe. Each patient was considered positive if they scored a high frequency of symptoms over the past 6 months and severity (based on the impact of the symptom on their quality of life) of ≥2 in each of the 6 categories. For neurologic/cognitive manifestations, patients were considered positive if they scored a high frequency over the past 6 months and severity of ≥43 (out of a maximum score of 100) using the CFQ. For category VI (other symptoms), patients were considered positive if they had a minimum of one persistent symptom from two of the autonomic, neuroendocrine, and immune manifestations for at least 6 months. All of our LC patients in both cohorts met the criteria for categories I, II, III, IV, and/or V, and VI [19–21]. Those LC patients who did not meet these criteria were excluded from the study.

The diagnosis of fibromyalgia (FM) was made based on new fibromyalgia diagnostic criteria proposed by ACR in 2010 [22–24]. This included the use of the Widespread Pain Index (WPI) and Symptom Severity (SS) scale which are indicators of symptom severity in patients with FM, and fulfill the case definition of FM. On the WPI scale, patients were considered positive if they had pain in 19 defined areas (score range: 0–19). The SS is comprised of two parts. Part 2a assesses the severity of fatigue, waking up unrefreshed, and cognitive symptoms using a 4-point Likert scale (score range: 0 to 9). In part 2b, patients

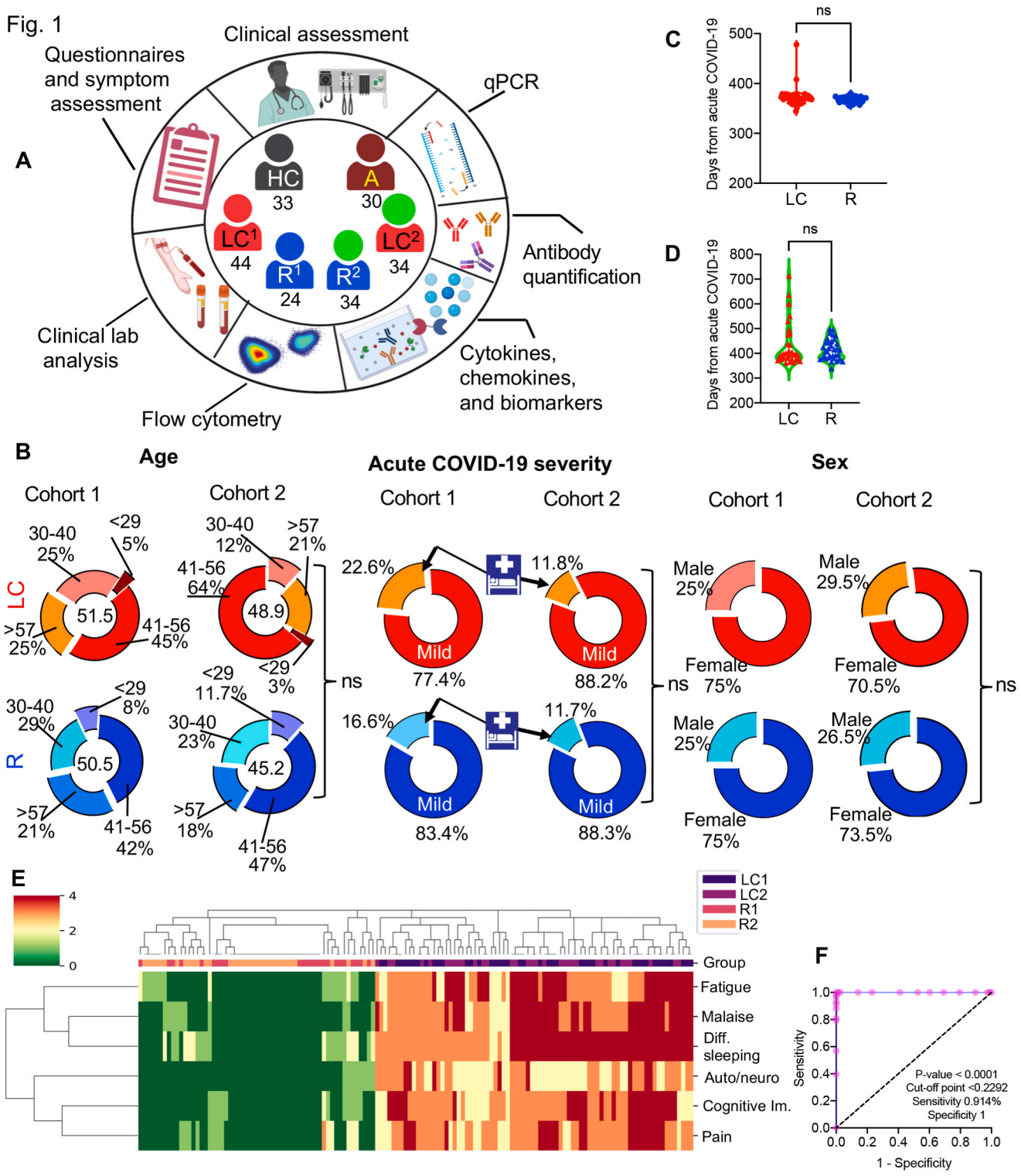

Fig. 1. Demographic and clinical analysis of LC cohorts. A, schematic of LC study design. Numbers in center of diagram indicate participants in each study cohort (HC = healthy controls with no prior-SARS-CoV-2 exposure/vaccination; A = acute SARS-CoV-2 infected and ICU-admitted; LC^1 = LC cohort 1 with persistent symptoms; R^1 = recovered cohort 1 without any symptoms; LC^2 = LC cohort 2 with persistent symptoms; R^2 = recovered cohort 2 without any symptoms). Outer ring indicates different studies/assays performed on patients/samples. B, Demographic characteristics for LC (top row, red) and R (bottom row, blue) displayed as ring charts. Centre values in "age" are median ages in years. Acute COVID-19 disease severity indicates percentages of patients with mild symptoms or required hospitalization in LC vs. R. C, Days from acute COVID-19 disease onset between LC and R in the first cohort, and D, the second cohort. E, Hierarchically-clustered heatmap of symptoms by Hamming distances and colored according to symptom severity score (seaborn). F, Receiver-operator curve (ROC) analysis of clinical score. Area under the curve (AUC) is reported with 95 % confidence intervals of AUC. *P* values were calculated using two tailed, Mann–Whitney *t*-test (B, C, D) and receiver operator characteristic curve analysis (F). Symbols in circle represents cohort 1 and in triangles indicates the cohort 2. The border color of green in plots represents the second cohort. Not significant (ns), difficulty (Diff.), impairment (Im.), autonomic/neuroendocrine (Auto/neuro).

report the presence or absence of 41 defined symptoms (fever, rash, seizures, dry eyes, etc.) and are scored 0 to 3 according to the number of symptoms (score of 0 = no symptoms, score of 1 = 1 to 10 symptoms, score of 2 = 11 to 24 symptoms, score of 3 = 25 or more symptoms). The sum of SS2a and 2b gives the SS score (score range: 0–12). The patients should either have a WPI $\geq$ 7 and SS $\geq$ 5, or a WPI between 3 and 6 and SS $\geq$ 9 for >6 months to diagnose FM diagnosis [22,23]. The CFQ was used to assess cognitive function [25]. The CFQ contains 25 items and uses a 5-Likert scale (0 = never; 1 = very rarely; 2 = occasionally; 3 = quite often; 4 = very often) to evaluate the frequency with which people experience failures in different areas of cognition such as perception, memory, and motor function. Scores are from (the range 0–100) with a score $\geq$43 indicating cognitive failure.

A similar process was used for the other questionnaires mentioned above. Collectively, our findings show that our cohort of LC patients present symptoms and criteria of ME/CFS and also suffer from FM and cognitive impairment.

2.2. Ethics statement

This study was approved by the Human Research Ethics Board (HREB) at the University of Alberta (protocol # Pro 00099502). A written informed consent form was obtained from all participants but a waiver of consent was obtained for those admitted to the ICU.

2.3. Cell isolation and culture

Peripheral blood mononuclear cells (PBMCs) were isolated using Ficoll-paque gradient methods (GE Healthcare). Cell cultures were performed in RPMI 1640 (Sigma-Aldrich) supplemented with 10 % FBS (Sigma-Aldrich) and 1 % penicillin/streptomycin (Sigma-Aldrich). In some experiments for performing intracellular cytokine staining (ICS), PBMCs were stimulated with the anti-CD3 (3 μg/ml) and anti-CD28 (1 μg/ml) antibodies and/or SARS-CoV-2 peptide pools (S and N) for 6 h in the presence of a Golgi blocker as described elsewhere [26,27]. For Gal-9-induced $CD8^+$ T cell activation, PBMCs were cultured without or with stimulation using anti-CD3/CD28 (3 μg/ml and 1 μg/ml, respectively) in the absence or presence of human recombinant Gal-9 (0.25 μg/ml, Gal Pharma). In other studies, to quantify Gal-9-induced cytokine production, PBMCs were cultured in the absence of any stimulation but with or without Gal-9 (0.25 μg/ml) overnight. For neutrophil-related studies, isolated neutrophils from fresh blood with the purity of >90 % were cultured in the absence or presence of LPS (2 μg/ml for 5 h). After this incubation time, neutrophils were subjected to further examination for the surface Gal-9 expression and ROS production. At the same time, culture supernatants were collected for soluble Gal-9 quantification by ELISA. In some experiments, total CECs, $CD45^+$/$CD45^-$CECs, immune cell lineages, and lightweight RBCs (LW/RBCs) were subjected to intracellular staining for ARTN according to our protocols for staining intracellular targets [28,29].

2.4. Proliferation assay

T cells were isolated and labeled with CFSE according to our protocols [29,30] and then cultured/stimulated with anti-CD3/CD28 for 3 days in the absence or presence of autologous enriched CECs at 1:1 or 1:05 ratios. Apocynin (1 mM, Sigma) was used to inhibit ROS production. However, N-acetyl-L-cysteine) did not inhibit CEC-mediated immunosuppression as reported elsewhere [31]. For these studies, total CECs were positively isolated from fresh PBMCs by using anti-CD71 biotinylated antibody followed by anti-biotin streptavidin linked magnetic beads (Miltenyi Biotect) with a purity of >95 % and as reported elsewhere [28,32]. Of note, CECs do not survive in freezing media and therefore must be studied/analyzed on freshly collected PBMCs.

2.5. Clinical tests

Complete blood count (CBC), whole blood antibody titers, CRP, RDW, and autoantibodies tests were performed at the clinical laboratory of the University of Alberta hospital.

2.6. Flow cytometry analysis

Fluorophore-labeled antibodies with specificity to human cell antigens and cytokines were purchased mainly from BD Biosciences, Thermo Fisher Scientific, BioLegend, and R&D. The following Abs were used in our study: anti-CD3 (SK7), anti-CD4 (RPA-T4), anti-CD8 (RPA-T8), anti-CD45RA (HL100), anti-CD45RO (UCHL1), anti-CD62L (DREG-56), anti-CCR7 (2-L1-A), anti-CD16 (B73.1), anti-CD15 (HI98), anti-CD45 (H-130 or 2D1), anti-VISTA (B7H5DS8), anti-TIM-3 (7D3), anti-PD-1 (MIH4), anti-CD160 (BY55), anti-CD244 (DM244), anti-Galectin-9 (9M1-3), anti-TIGIT (MBSA43), anti-CD39 (TU66), anti-CD73 (AD2), anti-CD19 (HIB19), anti-CD27 (O323), anti-CD38 (HIT2), anti-CD138 (MI15), anti-IgG (G18-145), anti-IgM (RMM-1), anti-HLA-DR (LN3), anti-TNF-α (MAB11), anti–IFN–γ (4S.B3), anti-CD71 (MA712), anti-ARTN (R&D, MAB2589), anti-CD235a (HIR2), anti-CD26 (M-A261), anti-CD161(HP-3G10), anti-TV α 7.2 (3C10), and anti-IL-18R α (H44). To exclude dead cells, live/dead staining (Thermo Fisher Scientific) was used. ROS staining on CECs and neutrophils was performed per the manufacturer's protocol (Sigma) [31]. The entire flow cytometry analyses were performed on freshly isolated PBMCs. For defining the gating strategy and antibody specificity, appropriate FMO (fluorescence minus one) and isotype control antibodies were used per the supplier's recommendation. To prevent variations, we used consistent flow cytometry panels with the same gating strategy for all study subjects, and a minimum of 100,000 events was acquired for each cell subset. Also, BD Biosciences CompBeads were used for control compensation. Following staining, cells were fixed and acquired on an LSRFortessa-SORP or Fortessa- X20 (BD Biosciences) and analyzed using the FlowJo software (version 10).

2.7. Cytokine and chemokine multiplex analysis and ELISA assays

Frozen samples at −20/80 °C were thawed and centrifuged for 15 min at 1500 g followed by dilution for quantifying cytokine and chemokine profiles, respectively. The concentration of cytokines and chemokines was quantified using the V-PLEX Neuroinflammation panel 1 kit (K15210D-1) from Meso Scale Discovery (MSD) [14,33]. This kit quantifies IL-1α, IL-1 β, IL-2, IL-4, IL-5, IL-6, IL-7, IL-8, IL-10, IL-12/IL23p40, IL-13, IL-15, IL-16, IL-17A, IFN-γ, TNF-α, TNF-β, Eotaxin-1, Eotaxin-3, MIP-1 α, MIP-1 β, Thymus- and activation-regulated chemokine (TARC), IP-10, MCP-1, MDC, MCP-4, VEGF (Vascular endothelial growth factor)-A, VEGF-C, VEGF-D, Tie-2 (endothelial-specific receptor, tyrosine kinase with immunoglobulin-like loops and epidermal growth factor homology domains 2), Flt-1, PlGF (placental growth factor), bFGF (basic fibroblast growth factor), SAA (serum amyloid A), CRP (C-reactive protein), ICAM-I and VCAM-1 according to the manufacturer's instruction. A total of 90 plasma samples from LC, R, and HCs were examined for these analytes. Data were acquired on the V-plex® Sector Imager 2400 plate reader. Analyte concentrations were extrapolated from a standard curve calculated using a four-parameter logistic fit using MSD Workbench 3.0 software.

The plasma Gal-9 concentration was quantified using the ELISA kit (R&D, DY 2045), similarly, TGF-β (R&D, DY240), ARTN (R&D, DY 2589), IL-6 (R&D, DY206), and TNF-α (R&D, DY210) were subjected to ELISA as we reported elsewhere [14,33,34]. The anti-CMV IgG was measured using the ELISA kit (abcam, ab1088724) and FABP-1 (R&D, Z-001).

2.8. Elispot assay

In brief, 1×10^5 (IFN-γ) PBMCs per well were stimulated with 2 μg/ml of the Spike (S) or nucleocapsid phosphoprotein (N) peptide pools (Miltenyi Biotec) of the Wuhan strain for 18 h according to our protocols [29]. Plates were developed using appropriate reagents (Mabtech) and acquired using the ImmunoSpot cell analyzer (Cellular Technology Limited (CTL), USA). A response was considered positive when the number of spot-forming cells (SFC) was twice the background and there were at least 20 spots per 1×10^6 PBMCs.

2.9. Gene expression assay

Total RNA was extracted from isolated total CECs from fresh PBMCs of LC patients with purity >95 % (Supplementary Fig. S9i) in TRIzol (Invitrogen) using the RNeasy Mini Kit (Qiagen). QuantiTect Reverse Transcription kit (Qiagen) was used to convert 1 μg RNA to cDNA, which was then subjected to quantitative PCR (qPCR). TaqMan PCR assays for each targeted gene were run in duplicates on CFX96 TouchTM Real-Time PCR Detection System (BioRad) Fold change in ARTN gene expression (Hs00754699_s1, Thermo Fisher Scientific) was calculated relative to CECs-depleted PBMCs according to our previous methods [29,35], where β-actin was used as a housekeeping gene.

2.10. Statistical analysis

The Wilks-Shapiro test assessed the distribution of data. The Mann-Whitney *U* test or Kruskal–Wallis analysis of variance (ANOVA) were used for non-normally distributed data. The Spearman correlation was calculated as a measure of linear association between two variables. Post hoc tests included Dunn's multiple comparisons for (Kruskal–Wallis analysis) and Tukey-Kramer test (one-way ANOVA with multiple comparisons). Measures are expressed as mean ± SEM and a *P*-value <0.05 was considered to be statistically significant. In violin plots, the middle line represents the median, the bottom line 1st quartile, and the top line 3rd quartile. No randomization was performed and no data points were excluded.

Significantly different parameters between LC and R were standardized for multivariable analysis. Heat maps were produced based on the Pearson correlation of pairwise complete observations with parameters ordered with hierarchical clustering. Multivariable regression of the LC vs R group was limited to the parameters with <30 % missing data and excluded $2B4^+CD160^+$ and $TIM\text{-}3^+CD160^+$ because they completely separated the LC/R groups. Multiple imputations (22) were used to impute data missing from any parameters. It is worth mentioning that all described parameters have the same direction and relatively the same magnitude in the final model for each dataset whether imputed or not.

Regularized logistic regression with an elastic net was used to identify the most important parameters using 10-fold cross-validation [36]and the ones that were the most important in at least 50 % of the imputations were selected for the final model. Ridge logistic regression determined the estimates of the most important parameters for each imputed dataset and these were averaged over imputations. We used ten-fold cross-validation to determine the best final model. While it might be typical to provide estimates with standard errors (and confidence intervals) in standard regression models, such values are not typically provided for penalized regression models [37]. Standard errors are not very meaningful for strongly biased estimates such as arise from penalized estimation methods and reporting a standard error can give a mistaken impression of great precision. Ordinarily, we would use the variables (aka biomarkers) selected by the elastic-net to fit a standard regression model and obtain estimates and associated standard errors (and confidence intervals). Unfortunately, we cannot take that approach because the number of variables selected by the elastic-net exceeds the number of variables that a standard regression model can fit with our sample size. Thus, we used the results of the elastic-net to 1) identify the variables that are the most important in discriminating between the LC and R groups and 2) to describe the relative importance of these variables by examining the sign and magnitude of the coefficient estimates. Analyses were conducted in R using the packages mice [38] and glmnet [39,40].

The PCA analysis was performed using logarithmic values of cytokines/chemokines upon normalization using Variance stabilized distribution (VSD). Then the PCA plot was generated using R script (R version 4.2.2).

3. Results

The cohort 1 (discovery cohort) comprised of 44 LC, individuals who had been infected with SARS-CoV-2 but recovered R, (n = 24) without any symptoms, healthy controls (HCs, whose samples were collected before the COVID-19 pandemic without exposure to SARS-CoV-2, n = 33, median age 49 ± 15.6), and acute COVID-19 (recruited from those with mild/moderate or severe disease in 2020 [14], n = 30, median age 66.13 ± 11.86) to multiple clinical visits and laboratory analyses (Fig. 1A–Supplementary Table S1). Similar analyses were performed in the second cohort, which was designed as a validating cohort. The cohort 2 consisted of (LC, n = 34) and (R, n = 34) (Fig. 1A–Supplementary Table S2). Initial demographic factors indicated that the LC and R groups were well-matched in age (median 51.5 ± 13.1 LC vs. 50.5 ± 13.3 R; cohort 1), (median 48 ± 9.8 LC vs. 45 ± 11.39 R; cohort 2), and proportion of hospitalized acute COVID-19 (22.6 % LC vs.16.6 % R; cohort 1) and (11.8 % LC vs. 11.7 % R; cohort 2) (Fig. 1B). Although LC and R cohorts were well-matched in sex (75 % female LC vs. 75 % female R; cohort 1) and (70.5 % female LC vs. 73.5 % female R; cohort 2), the odds of females having LC was 3 times higher than males in our cohorts (Fig. 1B). Analysis of elapsed days since the onset of SARS-CoV-2 acute infection revealed no significant difference between LC and R in cohort 1 (371 ± 19 days LC vs. 368 ± 6.2 days R) and cohort 2 (435 ± 89 days LC vs. 415 ± 40 days R) (Fig. 1C and D), further permitting direct comparison of persistent symptoms between LC and R. Co-morbidities in cohort 1 were 15.9 % and 16.6 % for LC and R, respectively. In cohort 2, co-morbidities were 8.8 % for LC and 5.8 % for R. All study subjects (LC and R) in the cohort 1 were SAS-CoV-2 vaccine-naïve and infected with the Wuhan Strain. However, 67.3 % of LC and 73.5 % of R were vaccinated in cohort 2 (Supplementary Tables S1 and 2) and this cohort was mainly infected with Delta and Omicron variants. Of note, 82.3 % and 76.4 % of LC and R in the second cohort were infected with SARS-CoV-2 before vaccination against this virus, respectively.

Analysis of the prevalence of symptoms using the DSQ [15,16] (methods section), which encompasses various domains present in patients with ME/CFS; namely: fatigue (I), malaise (II), sleep difficulties (III), pain (IV), neurological/cognitive manifestations (V), and other (VI) which include autonomic, neuroendocrine, and immune manifestations. Based on the CDC and WHO [15,16] guidelines, all of our LC patients met the criteria of ME/CFS. Analysis of the prevalence and severity of symptoms (I-VI) demonstrated a clustered and consistent pattern among LC and R in both cohorts (Fig. 1E, Supplementary Figs. S1A and B) without any difference between sexes (Supplementary Figs. S1C and D). To determine whether there was a pattern of symptoms associated with LC, scores were aggregated using a 5-point Likert scale (0–4 per each symptom for 6 categories; methods section). Considering the minimum inclusion score of ≥2/each symptom (methods section), the cumulative scores were (18.86 ± 2.9 LC vs. 2.29 ± 2.37 R; cohort 1) and (16.21 ± 1.6 LC vs. 1.38 ± 2.01 R; cohort 2) (Supplementary Figs. S1E and F). The receiver-operator curve analysis demonstrated a significant association of symptoms with LC (AUC = 0.914, CI 0.81–0.96) in both cohorts (Fig. 1F) or (AUC = 0.875, CI 0.69–0.95; cohort 1) and (AUC = 0.91, CI 0.81 to 0.96; cohort 2) (Supplementary Fig. S1G and H). It is worth mentioning that while these analyses can

provide insights into the extent of impairment, they are not meant to be used generating estimates of sensitivity and specificity for identifying ME/CFS. Additional analysis of the prevalence of symptoms among LC groups revealed frequent reports of fibromyalgia (72.7 %), inflammatory arthritis (20.4 %, all of which were on stable anti-rheumatic therapy and were followed by a rheumatologist), anxiety (20.4 %), and depression (13.6 %) in cohort 1. Similarly, fibromyalgia (67.6 %), depression (23.5 %), anxiety (23.5 %), and inflammatory arthritis (11.7 %), recorded in cohort 2, which is consistent with common symptoms reported in numerous LC cohorts.

To evaluate changes in the absolute number of immune cells, we performed a complete blood count. Compared to the R group, we detected a relative increase in absolute neutrophils and monocytes but a decrease in lymphocyte counts in the first LC cohort (Fig. 2A–D), which was reproduced in the second cohort (Fig. 2E–H). Considering the reduction in lymphocyte count in LC, we subjected their T, B, and NK cells to further analyses. Compared to the R group, we found a significant reduction in the absolute number of naïve (N) $CD4^+$ T cells in both LC cohorts (Fig. 2I and J) without any changes in the absolute number of central memory (CM) and effector memory (EM) cells in either cohort 1 (Supplementary Figs. S1I and J) or cohort 2 (Supplementary Figs. S1K and L). These observations were verified in fresh PBMCs of both cohorts (Fig. 2K, L, Supplementary Figs. S1M and N). Although the absolute number of effector T cells in the whole blood was not analyzed, we noted a significant expansion of terminal effector (TE) $CD4^+$ T cell subset in PBMCs of LC patients in both cohorts (Fig. 2K and L, Supplementary Fig. S2A). In the analysis of $CD8^+$ T cells, there was a significant decline in the absolute number of N T cells in the whole blood of both LC cohorts (Fig. 2M and N) without any changes in CM and EM T cells (Supplementary Figs. S2B–E). These observations were further confirmed in PBMCs of LC cohorts (Fig. 2O and P, Supplementary Figs. S2F and G). Moreover, a significant abundance of TE $CD8^+$ T cells in both cohorts was observed (Fig. 2O and P, Supplementary Fig. S2G) without any significant difference in the frequency of other subsets (Fig. 2P and Supplementary Fig. S2G). In light of the potential influence of cytomegalovirus (CMV) infection on T cell subsets (e.g. EM and TEMRA), we stratified our cohorts for this virus. However, the percentage of positive subjects for CMV IgG and CMV IgG titers were comparable in both cohorts (Supplementary Figs. S2H–K). Of note, we did not observe any significant difference in the absolute number of B cell subsets in the whole blood (Supplementary Fig. S2L-Q) and fresh PBMCs between the LC and R group in both cohorts despite the impact of acute SARS-CoV-2 infection on B cell phenotype and function [41] (Supplementary Fig. S2R-W). Likewise, NK cell count remained unchanged between LC and R in both cohorts (Supplementary Figs. S2X and Y). Our results suggest a dysregulated hematopoiesis, which skews towards myelopoiesis. Additionally, a reduction in naïve but expansion of TE T cells supports persistent T cell activation in LC patients.

Next, we subjected T cells to further analysis. Compared to the R group, we detected a significant increase in PD-1, TIM-3, CD160, CD244, TIGIT, and HLA-DR but reduction in CD73 expressing $CD8^+$ T cells in LC cohort 1 (Fig. 3A, Supplementary Fig. S3A). Almost the same results were observed in the second LC cohort (Fig. 3B). In $CD4^+$ T cells, PD-1, CD160, TIGIT, CD244, TIM-3, and VISTA expressing cells were significantly elevated in LC cohort 1 (Fig. 3C, Supplementary Fig. S3B), which was reproduced in cohort 2 (Fig. 3D). Comparison of T cells from LC with HCs revealed significant expansion of CD160, PD-1, TIM-3, CD39, TIGIT, CD38, and CD71 but reduction of CD73 expressing cells among $CD8^+$ T cells (Fig. 3E). Similarly, we found significant expansion of TIGIT, PD-1, CD244, CD160, CD71, CD38, and HLA-DR expressing cells among $CD4^+$ T cells in LC compared to HCs of cohort 1 (Fig. 3F). Of note, the R group $\geq$12 months post the onset of acute infection exhibited residual T cell activation evidenced by a significant elevation in the frequency of $CD8^+$ T cells expressing co-inhibitory receptors such as PD-1, CD39, and activation markers (e.g. CD38, CD71 and HLA-DR) (Fig. 3G). Likewise, $CD4^+$ T cells expressing PD-1, CD38, CD160, and CD71 were significantly enriched in LC compared to HCs in the first cohort (Fig. 3H). Moreover, we quantified the absolute number of $CD4^+$ and $CD8^+$ T cells expressing PD-1, TIM-3, VISTA, CD160, CD244, and TIGIT in PBMCs, which showed significant abundance of T cells expressing these co-inhibitory receptors in LC subjects of both cohorts (Supplementary Figs. S3C and D). Also, we found $CD8^+$ T cells co-expressing $2B4^+CD160^+$, $PD\text{-}1^+TIM\text{-}3^+$, $TIGIT^+TIM\text{-}3^+$, $2B4^+TIGIT^+$, and $TIGIT^+CD160^+$ were enriched in LC cohort 1 (Supplementary Fig. S3E–G), which was reproduced in cohort 2 (Supplementary Fig. S3H). Overall, our observations indicate the presence of markers of immune activation alongside upregulation of co-inhibitory receptors in T cells from LC patients. This reflects the presence of immune stimulus in these patients that promotes differentiation into TE cells to mount an immune response. Subsequently, the immune system initiates a regulatory mechanism to maintain immune homeostasis. However, such chronic immune activation may result in dysregulated and impaired T cells effector functions.

To determine the functionality of T cells expressing co-inhibitory receptors, we stimulated total PBMCs with SARS-CoV-2 peptide pools (e.g. S and N) [26]. The frequency of memory T cells to antigen-specific viral peptides as quantified by CD69, CD137, and CD154 [26,30] was extremely low to undetectable. To overcome this issue, we quantified antigen-specific T cell responses by IFN-γ Elispot assay [30]. We found a significantly lower response to the S peptide pool in LC than R in both cohorts (Supplementary Figs. S3I and J). Therefore, we decided to compare polyclonal effector functions (e.g. cytokine production) of T cells at the global level using anti-CD3/CD28 antibody stimulation. These analyses revealed a dichotomy for $TIM\text{-}3^+$ versus $PD\text{-}1^+CD8^+$ T cells in LC (Fig. 3I). While $TIM\text{-}3^+CD8^+$ T cells exhibited an impaired TNF-α/IFN-γ expression, $PD\text{-}1^+CD8^+$ T cells had greater TNF-α/IFN-γ expression levels compared to their negative siblings ($PD\text{-}1^-CD8^+$ T cells) within the same individual (Fig. 3I). Our multipronged analyses revealed that $CD8^+$ T cell exhaustion was selectively associated with TIM-3 and TIGIT but not PD-1 and 2B4 expression in cohort 1 (Fig. 3I-M, Supplementary Figs. S4A–F), which was verified in cohort 2 (Fig. 3N-Q, Supplementary Figs. S4G–J). These observations suggest impaired effector functions in the peripheral T cells in LC patients. However, whether some T cells, in response to stimuli (e.g., viral antigens) become tissue-resident in LC in unknown and should be taken into consideration.

To evaluate potential soluble factors associated with LC, we analyzed 40 analytes in the plasma of LC, R, and HCs. Pro-inflammatory cytokines/chemokines including IP-10, IL-12/IL-23p40, TNF-α, IL-1α, monocyte chemoattractant protein-1 (MCP-1), C-reactive protein (CRP), VCAM-1, placental growth factor (PlGF), IL-6, ICAM-1, VCAM-1, serum amyloid A (SAA) were significantly elevated in both LC cohorts (Fig. 4A and B, Supplementary Figs. S5A and B). In addition to the above-stated analytes, we found a significantly greater plasma level of IL-17, IFN-γ, MIP-1α, MDC, and IL-1β in the second cohort (Fig. 4B, and Supplementary Fig. S5B). In contrast, IL-16, Eotaxin-3 and vascular endothelial growth factor C (VEGF-C) were significantly reduced in both LC cohorts (Fig. 4A and B, Supplementary Figs. S5A and B). Principal component analysis (PCA) of plasma analytes clearly discriminated LC from R in both cohorts (Fig. 4C). Compared to HCs, eleven cytokines and chemokines (PlGF, MCP-1, IP-10, IL-12/IL23p40, IL-10, TNF-α, TNF-β, IL-6, VEGF soluble receptor (Flt-1), SAA, and CRP were significantly elevated in the plasma of LC cohort 1 but MCP-4, and VEGF-C were reduced (Supplementary Figs. S6A and A1). Finally, compared to HCs, eight analytes including TNF-α, Flt-1, IL-10, IL-7, IL-13, IL-15, IL-1α, and IL-1β were significantly higher in the R group while MCP-4, VEGF-D, and ICAM-1 were significantly reduced (Supplementary Fig. S6B and B1). Consistent with the plasma results, LC patients had significantly elevated levels of CRP in their whole blood in both cohorts (Supplementary Figs. S7A and B). Given the intestinal infection by SARS-CoV-2 [42], we detected increased plasma levels of intestinal fatty acid binding protein (I-FABP) in both LC cohorts (Supplementary Figs. S7C and D). This implies that compromised intestinal integrity and

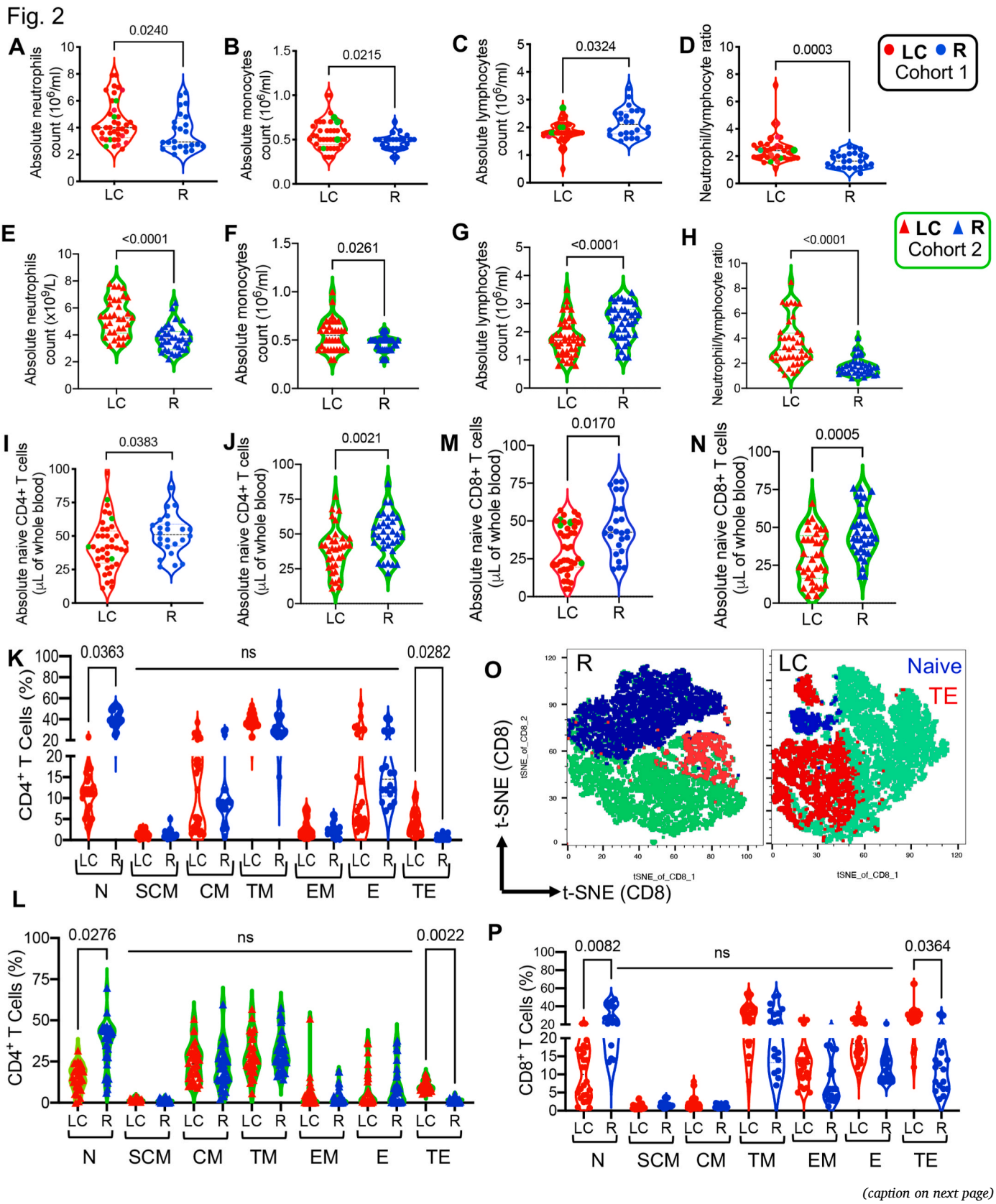

(caption on next page)

microbial/byproducts translocation may contribute to systemic inflammation in LC [43], however, merits further investigation. Notably, the plasma levels of TGF-β1 were significantly lower in the first LC compared to either the HC or R group (Supplementary Fig. S7E), which was further reproduced in the second cohort (Supplementary Fig. S7F). Hence, these observations suggest the presence of immune

Fig. 2. Distinct innate and adaptive immune cell phenotype in LC. A, Absolute number of neutrophils; B, Monocytes; C, Lymphocytes; D, Neutrophils to lymphocytes ratio in the whole blood of LC and R of the first cohort. E, Absolute number of neutrophils; F, Monocytes; G, Lymphocytes; H, Neutrophils to lymphocytes ratio in the whole blood of LC and R of the second cohort. I, Absolute number of naïve $CD4^+$ T cells in the whole blood of LC and R of cohort 1. J, Absolute number of naïve $CD4^+$ T cells in the whole blood of LC and R of cohort 2. K, Cumulative data of $CD4^+$ T cells including naïve (N), stem cell memory (SCM), central memory (CM), transitional memory (TM), effector memory (EM), effector (E), and terminal effector (TE) in peripheral blood mononuclear cells (PBMCs) of L and R of cohort 1. L, cumulative data of $CD4^+$ T cells (e.g. N, SCM, CM, TM, EM, E, and TE) in PBMCs of L and R of cohort 2. M, Absolute number of naïve $CD8^+$ T cells in the whole blood of LC and R in cohort 1. N, Absolute number of naïve $CD8^+$ T cells in the whole blood of LC and R in the cohort 2. O, Representative $CD8^+$ T cell tSNE plots from a LC patient and a R participant for N and TE cells. P, Cumulative data of $CD8^+$ T cells (e.g. N, SCM, CM, TM, EM, E, and TE) in PBMCs of L and R in cohort 1. *P* values were calculated using two tailed, Mann–Whitney *t*-test (A–J, M, N) or Kruskal–Wallis analysis with Dunn's multiple comparisons test (K, L, P). Green colored dots represent ICU-admitted LC patients in the first cohort. The blue symbol represents recovered (R) and red (LC). Symbols in circle and triangles represent cohorts 1 and 2, respectively. The border color of green in plots represents cohort 2. Not significant (ns).

activation/dysregulation in LC patients.

Expression of galectin-9 (Gal-9), which has an immunomodulatory role in acute COVID-19 disease [14], HIV infection [34,44], and other inflammatory conditions [45–47] was significantly elevated in the plasma of LC compared to both HCs and R in our first cohort (Fig. 4D) and the second cohort (Fig. 4E).

To determine whether plasma Gal-9 level has any predictive value for LC, we compared the plasma levels of Gal-9 in a subset of LC patients with those in the R group at the acute phase of the disease. These patients were recruited, and their plasma samples were collected at the acute stage of disease [14]. We identified that 13 of our LC patients belonged to our previous acute phase cohort, and similarly, we were able to recruit 17 individuals from the R group of the same cohort. However, these analyses revealed comparable Gal-9 levels in LC and R at the acute phase of COVID-19 disease (Supplementary Fig. S7G).

Although the main source of Gal-9 is unknown, it can be secreted via unknown mechanisms by both immune and non-immune somatic cells [48]. Subsequently, Gal-9 via interaction with different receptors exhibits a wide range of immunomodulatory properties [14,27,49]. In agreement, we found that recombinant Gal-9 enhances $CD8^+$ T cell activation as evidenced by the upregulation of CD38/HLA-DR in HC and R participants but dampens the proportion of $CD8^+$ T cells expressing CD38/HLA-DR in LC patients of cohort 1 (Supplementary Figs. S7H–K). A similar pattern was observed in $CD8^+$ T cells from R and LC participants in the second cohort (Supplementary Figs. S7L and M). The differential effects of Gal-9 on $CD8^+$ T cells from LC might be related to a higher proportion of $CD8^+$ TIM-3^+ T cells from LC patients [30] (Fig. 3A and B). Although Gal-9 transiently induces T cell activation, its prolonged interaction with T cells impairs their effector functions [50,51]. Considering the potential stimulatory role of Gal-9 upon interaction with innate immune cells during acute SARS-CoV-2 and HIV infection [14,52,53], we found that recombinant Gal-9 promotes IL-6 and TNF-α production by PBMCs of HCs, R, and LC participants in the first cohort (Supplementary Fig. S7N and O), which was reproduced in the second cohort (Supplementary Fig. S7P and Q). Of note, Gal-9 exerted a more pronounced stimulatory effect in PBMCs from LC than R participants in both cohorts (Supplementary Fig. S7N-Q). This could be linked to the relative abundance of monocytes and possibly their activation status in LC. These observations suggest that Gal-9 may contribute to immunomodulation in LC as reported in other conditions [14,30,52,53].

In line with this hypothesis, multiple variable analysis confirmed a positive correlation between the plasma Gal-9 levels with MIP-1β, CRP, and IL-10 in cohort 1 (Supplementary Fig. S7R). Intriguingly, a similar pattern was observed for the correlation of Gal-9 with these analytes plus VCAM-1 in cohort 2 (Supplementary Fig. S7S).

In agreement with previous reports that activated neutrophils shed Gal-9 in acute COVID-19 disease and HIV infection [14,52,54], we observed scarce surface Gal-9 expression in neutrophils from LC patients (Supplementary Figs. S8A and B). This activation phenotype upon Gal-9 shedding was confirmed by a significant elevation in reactive oxygen species (ROS) production in neutrophils from LC patients than R (Supplementary Figs. S8C and D). The shedding of Gal-9 and subsequently enhanced ROS production was further validated upon stimulation of neutrophils [52] from R participants with LPS (2 μg/ml for 5 h) (Supplementary Figs. S8E–I). A sharp decline in surface expression but an increase in soluble Gal-9 in culture supernatants confirms the shedding of Gal-9 by activated neutrophils (Supplementary Figs. S8E–G). These results suggest an activated neutrophil phenotype may contribute to the elevation of plasma Gal-9 in LC as reported in other chronic inflammatory settings (e.g. rheumatoid arthritis) [45,47].

Given the susceptibility of mucosal-associated invariant T (MAIT) cells to Gal-9 induced apoptosis [55], we found their frequency was significantly declined in both LC cohorts (Supplementary Fig. S8 J-M). MAIT-like cells defined as $CD26^{high}CD8^+$ T cells express semi-invariable T-cell receptor-α chain (TCR-α) composed of TV α 7.2, CD161, and IL-18Rα [56,57] (Supplementary Fig. S8N–P). Our further investigations revealed that MAIT cells from LC patients were highly prone to Gal-9 induced apoptosis when treated with this lectin (0.25 μg/ml) overnight (Supplementary Figs. S8Q and R). As a result, Gal-9 treatment significantly reduced the proportion of viable MAIT cells (Supplementary Figs. S8S and T). Consistent with these results, we found a moderate but significant inverse correlation between the plasma levels of Gal-9 and the frequency of MAIT cells in both LC cohorts (Supplementary Figs. S8U and V). However, we observed that MAIT cells from the R group were not susceptible to Gal-9 induced apoptosis (Supplementary Fig. S8W). Consequently, we did not find any correlation between the plasma levels of Gal-9 and the proportion of MAIT cells in both R cohorts (Supplementary Figs. S8X and Y). To delineate the mechanism behind the increased susceptibility of MAIT cells from LC patients to Gal-9-induced apoptosis, we conducted additional studies. Considering the reported role of Gal-9 induced apoptosis of $CD8^+$ T cells through interaction with TIM-3 [34,58], we examined the expression of TIM-3 in MAIT cells from both LC and R individuals. These investigations revealed significantly higher levels of TIM-3 expression in MAIT cells from LC patients compared to their counterparts in the R group (Supplementary Fig. S8Z and Z1). To determine whether blocking Gal-9: TIM-3 interactions could prevent Gal-9 induced MAIT cells apoptosis, we cultured PBMCs from both LC and R groups in the absence and absence of lactose (30 mM) [34]. These studies demonstrated that lactose-mediated blockade of Gal-9: TIM-3 interactions prevented the reduction in the proportion of MAIT cells in LC but not in the R group (Supplementary Figs. S9A–C). In line with these findings, we found that lactose efficiently mitigated Gal-9-induced apoptosis in MAIT cells from LC patients (Supplementary Fig. S9D). These observations imply an important immunomodulatory role for Gal-9 in LC.

Next, we hypothesized that dysregulated erythropoiesis and subsequently low-grade hypoxia might be a potential mechanism associated with the fatigue syndrome observed in LC patients [59,60]. Under normal physiological conditions, RBCs are generated in the bone marrow and their immature counterparts are absent or scarce in the blood circulation of humans [61,62]. However, under pathological conditions or stress hematopoiesis, erythroid progenitors/precursors ($CD71^+$ erythroid cells (CECs)) become abundant in the peripheral blood [61–63]. This has already been reported in acute COVID-19 patients [59,64]. In support of this hypothesis, we found a significant expansion of CECs in the peripheral blood of LC compared to HCs and R individuals in our first cohort (Fig. 4F and G, Supplementary Fig. S1M). This was further verified in the second cohort (Fig. 4H). In agreement

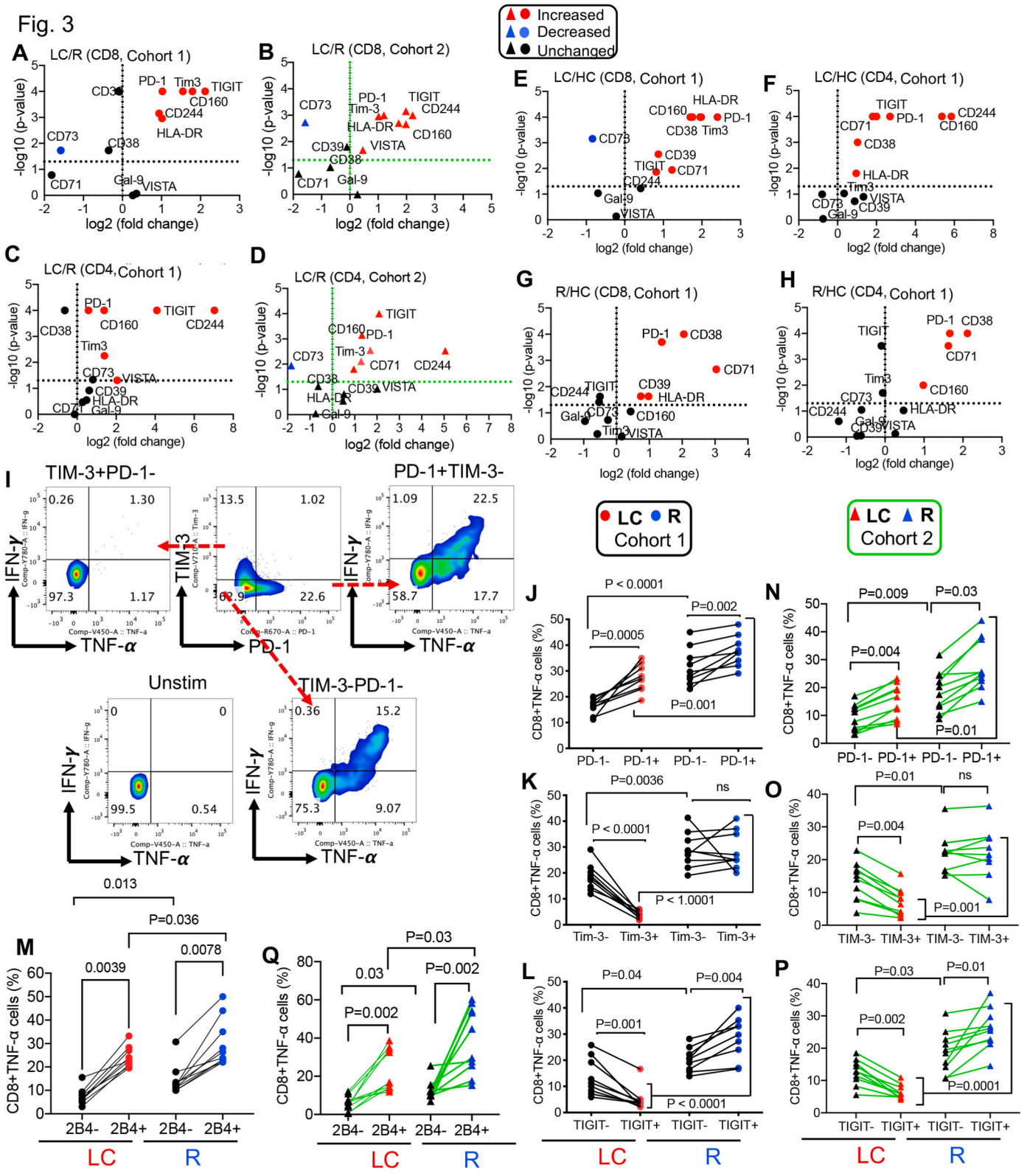

(caption on next page)

with the observed unusual morphological abnormalities of RBCs in acute COVID-19 patients [65], we noted a significant increase in the absolute number of RBC distribution width (RDW) in the whole blood of LC compared to the R group of both cohorts (Fig. 4I and J). Elevated RDW is linked to >6 times increased mortality risk in COVID-19 patients [65]. This abnormality was further bolstered by the abundance of $CD235a^{+}CD71^{-}$ CECs or lightweight (LW) RBCs in PBMCs of LC patients (Fig. 4H) as reported in acute COVID-19 [59]. Overall, these results

Fig. 3. The upregulation of co-inhibitory receptors and selective T cell exhaustion distinguishes LC. A, Volcano plot illustrating the magnitude and significance of increase in percentages of PD-1, CD160, TIM-3, CD244, TIGIT, and HLA-DR but decreased percentages of CD73 expressing $CD8^+$ T cells in PBMCs of LC vs R in cohort 1. B, Volcano plot illustrating the magnitude and significance increase in percentages of PD-1, TIM-3, CD160, CD244, TIGIT, HLA-DR, and VISTA but decreased percentages of CD73 expressing $CD8^+$ T cells in PBMCs of LC vs R in cohort 2. C, Volcano plot illustrating the magnitude and significant increase in percentages of PD-1, CD160, TIGIT, CD244, TIM-3 and VISTA expressing $CD4^+$ T cells in PBMCs of LC vs R in cohort 1. D, Volcano plot illustrating the magnitude and significant increase in percentages of PD-1, TIGIT, CD160, CD244, TIM-3, and CD71 expressing $CD4^+$ T cells in PBMCs of LC vs R in cohort 2. E, Volcano plot illustrating the magnitude and significant increase in percentages of PD-1, CD160, HLA-DR, TIM-3, CD38, CD39, CD71, TIGIT, and CD244 expressing $CD8^+$ T cells in PBMCs of LC vs HC in cohort 1. F, Volcano plot illustrating the magnitude and significant increase in percentages of PD-1, CD160, CD244, TIGIT, CD71, HLA-DR, and CD38 but CD73 expressing $CD4^+$ T cells in PBMCs of LC vs HC in cohort 1. G, Volcano plot illustrating the magnitude and significant increase in percentages of PD-1, CD38, CD71, CD39 and HLA-DR expressing $CD8^+$ T cells in PBMCs of R vs HC in cohort 1. H, Volcano plot illustrating the magnitude and significant increase in percentages of PD-1, CD71, CD160, and CD38 expressing $CD4^+$ T cells in PBMCs of R vs HC in cohort 1. I, Representative flow cytometry plots of IFN-γ and TNF-α expression in TIM-3^+ and PD-1^+ $CD8^+$ T cells compared to their negative counterparts in PBMCs from a LC patient either unstimulated (Unstim) or stimulated (Stim) with anti-CD3/CD28 antibodies for 6 h. J, Cumulative data of TNF-α expression in PD-1^+ and PD-1^-CD8^+ T cells; K, Cumulative data of TNF-α expression in TIM-3^+ and TIM-3^-CD8^+ T cells; L, Cumulative data of TNF-α expression in $TIGIT^+$ and $TIGIT^-CD8^+$ T cells; M, Cumulative data of TNF-α expression in CD244 $(2B4)^+$ and $2B4^-CD8^+$ T cells in stimulated PBMCs with anti-CD3/CD28 antibodies from LC and R of cohort 1. N, Cumulative data of TNF-α expression in PD-1^+ and PD-1^-CD8^+ T cells; O, Cumulative data of TNF-α expression in TIM-3^+ and TIM-3^-CD8^+ T cells; P, Cumulative data of TNF-α expression in $TIGIT^+$ and $TIGIT^-CD8^+$ T cells; Q, Cumulative data of TNF-α expression in CD244 $(2B4)^+$ and $2B4^-CD8^+$ T cells in stimulated PBMCs with anti-CD3/CD28 antibodies from LC and R of cohort 2. *P* values were calculated using two tailed, Mann–Whitney *t*-test (A-H) or Wilcoxon matched-pairs two-tailed *t*-test (J–Q). Not significant (ns). Circles or triangles (A–H) marked in red and blue are significantly increased or decreased, respectively. The circles in black show no significant difference. Unstimulated (unstim).

suggest the presence of dysregulated erythropoiesis in LC.

A majority of patients with LC in our cohort suffered from co-morbid fibromyalgia and cognitive dysfunction. Given the role of artemin (ARTN) in inflammatory pain and neuron function [66,67], we found a significant elevation of this neurotrophic factor in the plasma of the first LC cohort (Fig. 4K), which was reproduced in the second cohort (Fig. 4L). With this in mind, it is important to identify the potential source(s) of elevated ARTN in LC. ARTN is secreted along blood vessels, in cells near sympathetic axonal projections [68,69], and by CECs in tumor models [70,71]. We detected ARTN mRNA and protein in total CECs of LC in cohort 1 (Fig. 5A, Supplementary Figs. S9E and F), which was verified at the protein level in cohort 2 (Fig. 5B and D). In particular, ARTN expression was significantly greater in $CD45^+$CECs than $CD45^-$ subset (Fig. 5B and D). In agreement with this observation, we identified a moderate positive correlation between the frequency of $CD45^+$CECs, which are defined as the most potent subpopulation of CECs [61,72] and plasma ARTN levels in both LC cohorts (Supplementary Figs. S9G and H). Interestingly, we observed that CECs from the R group expressed negligible levels of ARTN (Supplementary Fig. S9I). Consequently, we did not find any correlation between plasma levels of ARTN and the frequency of $CD45^+$CECs in R individuals from both cohorts (Supplementary Figs. S9J and K). Moreover, we found $CD45^+$CECs as a potential source of ROS in LC patients (Supplementary Figs. S9L and M). While total CECs have lower ROS levels than neutrophils, their $CD45^+$ counterparts produce significantly higher ROS compared to CD15 cells in LC patients (Supplementary Figs. S9M and N). However, its noteworthy that $CD45^+$CECs from the R group produce significantly lower levels of ROS than their counterparts in LC patients (Supplementary Fig. S9O). To delineate the role of CECs in LC, we examined $CD8^+$ T cells proliferation in the presence of enriched CECs from PBMCs of LC patients (Supplementary Fig. S9P). These studies revealed that CECs in a dose-dependent manner impair T cell proliferation *in vitro* (Supplementary Figs. S9Q and R). Of note, apocynin partially but significantly abrogated CEC-mediated immunosuppression of T cells (Supplementary Figs. S9Q and R) as reported elsewhere [31,32]. It's likely that CECs in addition to ROS via arginase I/II exert their immunosuppressive functions [62]. The abundance of $CD45^+$CECs in both LC cohorts (Supplementary Figs. S9S and T), suggest that CECs may play contribute to T cell impairment, possibly through ROS production, in LC patients. Although isolating CECs from PBMCs of the R group was impractical due to their very low frequency, our data clearly demonstrate that CECs from the R group express negligible levels of ARTN and ROS (Supplementary Figs. S9I and L). Therefore, these observations indicate that not only are CECs abundant in LC patients, but they also have differential properties compared to their counterparts in the R group. Furthermore, we detected a higher Gal-9 expression in CECs versus LW/RBCs (Supplementary Figs. S9U and V). It is worth mentioning that permeabilization buffers unlike other immune cells compromise human but not mouse CECs' cell membrane. Nevertheless, CECs in LC have a more rigid cell membrane particularly their progenitors ($CD45^+$) as reported for acute COVID-19 [73]. This characteristic enabled us to quantify intracellular ARTN in CECs in LC patients. ARTN plays a neuroprotective role and is associated with inflammatory bone pain [69,74], and its elevation may contribute to symptoms associated with LC. To this end, we found a positive correlation between the plasma ARTN levels with the pain symptoms severity (SS), widespread pain index (WPI) (Fig. 5E), and cognitive failure score (Fig. 5F) in the first cohort, which was fully verified in the second cohort (Fig. 5G and H). Collectively, our observations support a potential role for dysregulated erythropoiesis associated with ARTN in LC.

Next, we analyzed total blood antibody levels and the presence of different autoantibodies. Compared to the R group, we did not observe any difference in total IgG, IgA, IgM, IgE, IgG1, IgG2, and IgG3 in our first cohort except a lower IgG4 (Supplementary Fig. S9W). Consistently, no significant difference in antibody titers was observed in the second cohort (Supplementary Fig. S9X). Interestingly, we observed a significant decrease in diphtheria antitoxin levels in both LC cohorts (Supplementary Fig. S9Y) but tetanus antitoxin and anti-rubella IgG levels remained the same between LC and R in both cohorts (Supplementary Fig. S9Z and Z1). In agreement with previous reports [75,76], we found the presence of autoantibodies in 54.5 % of our first LC cohort. Among the detected autoantibodies, antinuclear antibodies (ANA), anti-ribonucleoprotein (anti-RNP), and nuclear antigen antibodies (ENA) were the most frequently present (37.44 %) followed by IgG rheumatoid factors (33.28 %), and cyclic citrullinated peptide (anti-CCP), perinuclear anti-neutrophil cytoplasmic antibody (pANCA), myeloperoxidase antineutrophil cytoplasmic antibodies (MPO-ANCA) (16.64 %), while anti-mitochondrial (8.32 %) and anti-thyroid peroxidase (anti-TPO, 4.14 %) were the least in the first LC cohort (Supplementary Fig. S9Z2). This was confirmed in approximately 55.8 % of the second LC cohort (Supplementary Fig. S9Z3). However, autoantibodies were scarce in the R (Supplementary Fig. S9Z4) and undetectable in HC cohorts.

Finally, we performed multivariable analysis on 39 major parameters that were standardized. The strength of Pearson correlation between parameters segregated 23 elevated and 16 reduced parameters in LC vs. R in both cohorts (Supplementary Figs. S10A and B). We identified physiologically expected correlations (e.g. CRP with SAA and CD8 TE with exhausted T cells) and novel and less explored relationships such as a positive correlation between Gal-9 with CRP, VCAM-1, IL-10, and IP-10 as well as Gal-9 with lower cytokine production capacity of TIM-3 and TIGIT expressing $CD8^+$ T cells (Fig. 5I, Supplementary Figs. S10C and D). These results validate our observations that elevated Gal-9 may contribute to the suppression of adaptive but activation of innate immune cell effector functions (Supplementary Fig. S7H–Q). As a further

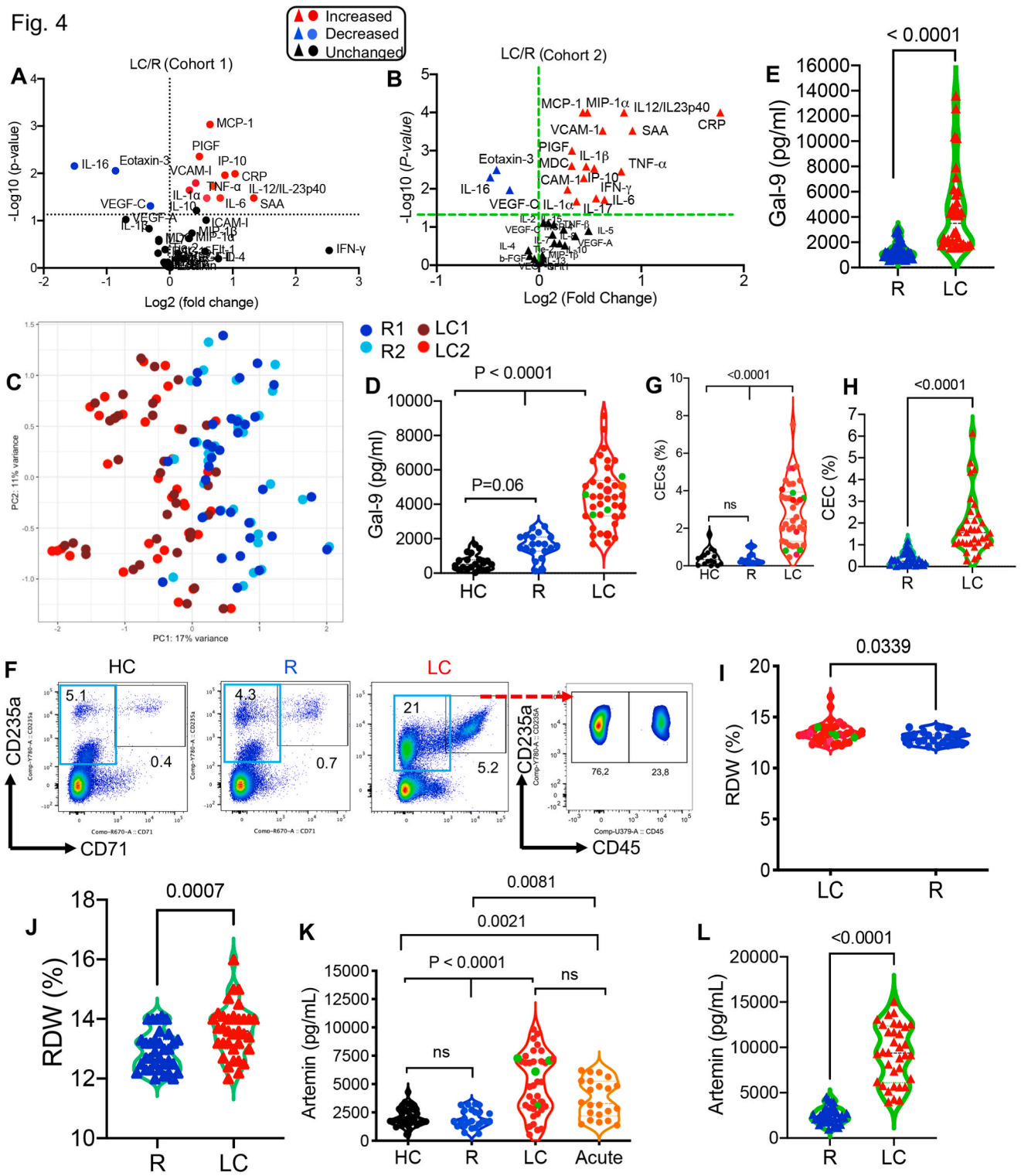

Fig. 4. Elevated levels of proinflammatory cytokines, chemokines, and Gal-9 in LC patients A, Volcano plot illustrating the magnitude and significance increase in MCP-1, PlGF, VCAM-1, ICAM-1, IP-10, CRP, TNF-α, IL-1α, IL-6, IL-12/IL-23p40, SAA but decrease in IL-16, VEGF-C and Eotaxin-3 in plasma samples of LC vs R in the first cohort. B, Volcano plot illustrating the magnitude and significance increase in MCP-1, PlGF, VCAM-1, ICAM-1, IP-10, CRP, TNF-α, IL-1α, IL-6, IL-12/IL-23p40, SAA, IL-17, MD, and IFN-γ but decrease in IL-16, VEGF-C and Eotaxin-3 in plasma samples of LC vs R in the second cohort. C, Principal component analysis (PCA) was performed to show the distribution of plasma analytes from the combination of two LC and two R groups (dark red, LC1, cohort 1 and red LC2, cohort 2 vs. dark blue R1, cohort 1 and light blue R2, cohort 2), each dot represents a study subject. D, The plasma Gal-9 concentrations in HC, R and LC of the first cohort and E, R and LC of the second cohort. F, Representative flow cytometry plots; G, cumulative data of percentages of total CECs in HC, R and LC of the first cohort and H, in R and LC of the second cohort. I, The percentage of RDW in the whole blood of LC vs R of the first cohort and J, in R and LC of the second cohort. K, Concentration of plasma ARTN in HC, R, LC and acute COVID-19 patients in the first cohort and L, R and LC in the second cohort. Circles or triangles marked in red and blue are significantly increased or decreased, respectively. The squares in black show no significant (ns) difference. *P* values were calculated using two tailed, Mann-Whitney *t*-test for (A, B, E, H, I, J, L), Kruskal–Wallis analysis with Dunn's multiple comparisons test (D, G, K).

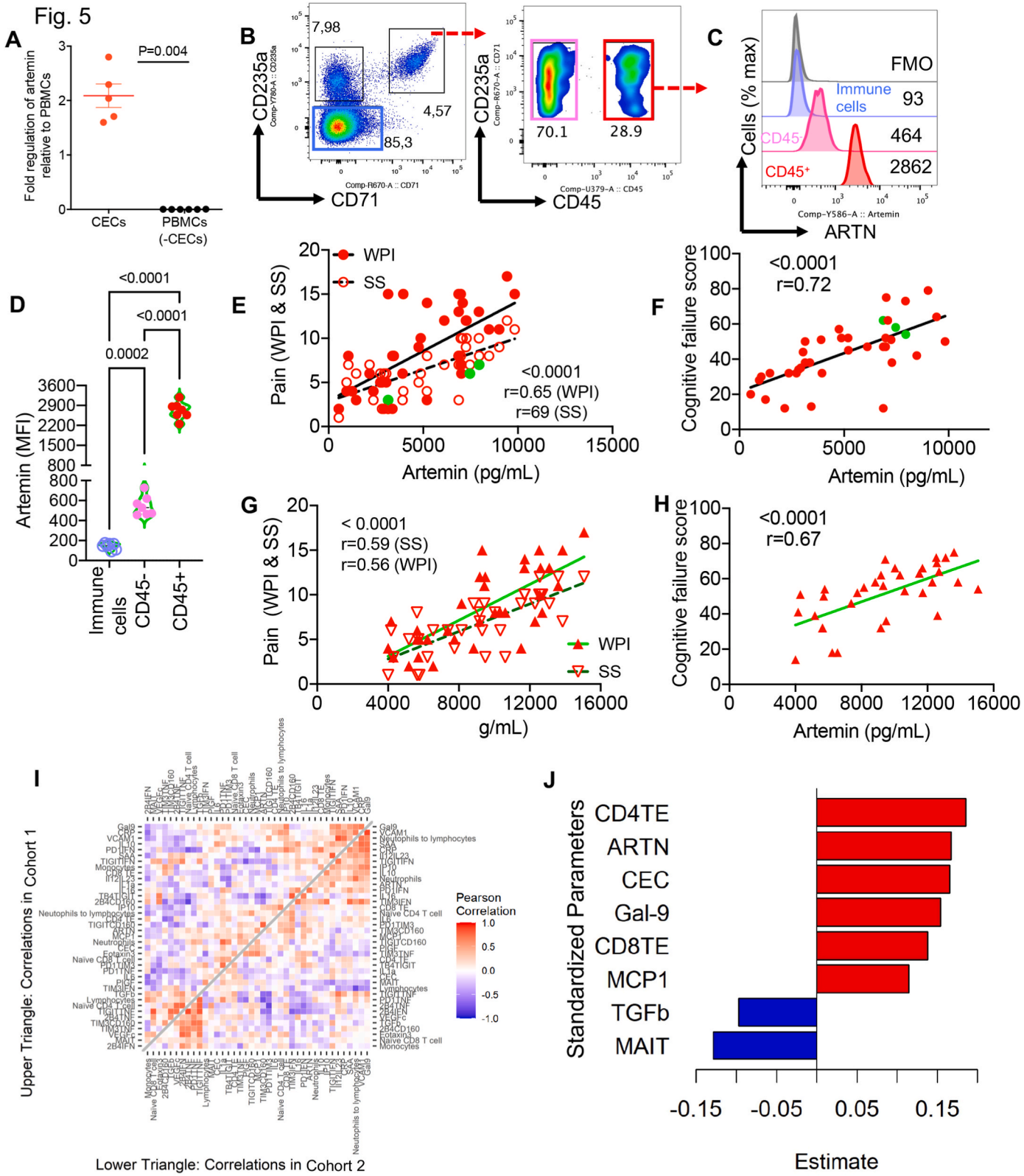

Fig. 5. CECs a potential source of increased plasma ARTN levels in LC patients. A, ARTN mRNA expression in total CECs vs all other immune cell lineages. B, Representative flow cytometry plots of CECs ($CD45^{-}$ vs $CD45^{+}$). C, Representative plots of the intensity of ARTN expression in each indicated subset. D, Cumulative data of the mean fluorescence intensity (MFI) of ARTN in immune cell lineages, $CD45^{-}$, and $CD45^{+}$CECs. E, The positive correlation between the plasma ARTN levels with the pain symptom severity (SS) score, the widespread pain index (WPI), and F, cognitive failure score in LC of the first cohort. G, The positive correlation between the plasma ARTN levels with the pain symptom severity (SS) score, the widespread pain index (WPI), and H, cognitive failure score in LC of the second cohort. I, the heatmap of Pearson correlation of standardized parameters for LC in both cohorts. J, Estimates of standardized parameters from the regularized logistic regression model. *P* values were calculated using two tailed, Mann-Whitney *t*-test (A), ANOVA (D) and the Spearmen correlation analysis (E–H). Pearson correlation and logistic regression (I, J).

method of probing the correlation structure, we conducted hierarchical clustering using a basic distance metric divided from the full pairwise Pearson correlation matrix on the set of 39 parameters in R and LC of both cohorts (Supplementary Figs. S10E and F). These analyses reinforced expected parameters such as co-inhibitory receptors, CD4/CD8 TE, ARTN, Gal-9, CEC, and neutrophils in one cluster. An unexpected and novel finding was the grouping of ARTN with TIGIT, TIM-3, CD160, PD-1, and 2B4 co-expressing $CD8^+$ T cells in LC. There is no clear evidence for the connection between ARTN and co-inhibitory receptors in T cells since we were unable to detect ARTN receptor (GFRα3) in T cells. Nevertheless, further studies are needed to shed light on this connection. Interestingly, monocytes and IL-6 formed a subgroup, and other soluble analytes (e.g. CRP, SAA, IL-10, VCAM-1 IP-10, MCP-1, and IL-12/13) clustered together in both LC cohorts. In contrast, the reduced cytokine production capacity of $CD8^+$ T cells expressing different co-inhibitory receptors was grouped with the proportion of MAIT, lymphocyte, and naïve T cells in LC patients (Supplementary Figs. S10E and F). Further, we used regularized logistic regression methods to distinguish the LC from the R group as a function of multiple standardized parameters. Since values of TIM-3^+CD160^+ and 2B4^+CD160^+ $CD8^+$ T cells completely separated the LC/R groups (Supplementary Fig. S10G), they were not included in the multiple regression model. This model revealed that the increase in CD4TE, ARTN, CEC, Gal-9, CD8TE, and MCP1 but the decrease in TGF-β1 and MAIT cells can distinguish LC from R (Fig. 5J). Of note, we used elastic-net regularized generalized linear regression model [39]. This type of penalized regression model is quite different from standard regression models. While it might be typical to provide confidence intervals in standard regression models, such values are not typically provided for penalized regression models.

4. Discussion

LC is emerging a significant global health concern. We conducted comprehensive immune-profiling and functional assays on two independent cohorts of LC with ME/CFS, R, and HCs to advance our understanding of the pathophysiology of LC. Overall, our results demonstrate diverse immunological alterations in LC patients. The existence of relatively reduced lymphocytes but increased neutrophils, monocytes, and CECs even 12 months after acute SARS-CoV-2 infection suggest a dysregulated or impaired hematopoiesis. Mechanistically, microbial products and the consequences of SARS-CoV-2 infection-induced mediators (e.g. cytokines, chemokines, and growth factors) can have a prominent impact on hematopoietic stem and progenitor cells [73]. Lingering dysregulated hematopoiesis in LC suggests a potentially impaired antiviral response and/or increased innate immune response (e.g. cytokines, chemokines, and Gal-9). Subsequently, an impaired antiviral response may increase antigen persistence and promote chronic inflammation, which contributes to the upregulation of co-inhibitory receptors. Therefore, prolonged antigenic stimulation may also enhance T-cell differentiation into effector and terminal effectors. This was supported by a significant reduction in naïve T cells but an increase in terminal effector T cells in LC patients, as reported elsewhere [7]. Alternatively, chronic T cell activation may result in T cell exhaustion, as reported in other LC cohorts [77,78]. Strikingly, we observed a significant elevation in the plasma Gal-9 in LC patients. This elevation has been noted in the acute stage of SARS-CoV-2 infection [14]. Gal-9, as a potent immunomodulatory protein, can interact with different receptors on different immune cells, such as TIM-3, CD44, TCR, CD137, PD-1, etc [44,48,52]. This interaction may result in T cell exhaustion or apoptosis (e.g. TIM-3), immune cell activation (e.g. monocytes, NK cells, and macrophages), and induction of proinflammatory mediators [14,50,53]. In agreement with our observations, a recent study has highlighted T cell dysregulation, systemic inflammation, and a lack of coordination between SARS-CoV-2 specific B and T cells in patients with LC [78]. Although hyperinflammation in the acute phase and viral reactivation (e.g. EBV and CMV) are considered contributing factors to LC [76], our findings did not support a role for CMV and inflammatory milieu during the acute stage of disease, as indicated by Gal-9 levels, in relation to the onset of LC. We also found that circulating neutrophils in LC patients exhibit an activated phenotype, suggesting an altered metabolic profile and potentially impaired capacity to respond to signals from other immune cells [79]. Consistent with the proposed evidence of hematological system alterations, such as anemia and thrombocytopenia [80,81], we observed a significant expansion of CECs in the peripheral blood of LC patients. CECs due to their immunosuppressive properties may suppress T cell response against SARS-CoV-2 antigens as reported in acute infection [59]. Alternatively, CECs and activated neutrophils, acting as potential sources of ROS, may contribute to oxidative stress as a contributing factor to the development and progression of LC [82,83]. Previous studies have demonstrated that CECs express ARTN [70]. Given the role of this neurotrophic factor in osteoarthritis pain and our observed direct correlation between the pain indexes and ARTN levels, we propose that the elevated levels of ARTN may contribute to the pain symptoms associated with LC. Furthermore, the association between plasma ARTN levels and cognitive impairments score in LC patients suggests a potential role for ARTN in LC pathogenesis. However, whether the elevated levels of ARTN in LC function pathologically or act as a compensatory mechanism to repair neural damage [84] needs further investigation.

One of our notable findings is that females are significantly more prone to experience LC than males, a trend reported in other cohorts as well [85,86]. This sex disparity may be attributed to the potentially more robust innate and adaptive immune responses in females compared to males, rendering them susceptible to autoimmune-related conditions. In line with this observation, we detected autoantibodies in over 50 % of our LC patients, consistent with findings from other research groups [75].

Finally, our regularized logistic regression analysis validated that the expansion of TIM-3^+CD160^+ and 2B4^+CD160^+ $CD8^+$ T cells serves as a reliable discriminator between the LC and R groups.

Consistent with our broader findings, the regression model further confirmed that an increase in CD4TE, ARTN, CEC, Gal-9, CD8TE, and MCP1, coupled with a decrease in TGF-β1 and MAIT cells, effectively distinguishes LC with ME/CFS from the R groups.

5. Conclusions

Consequently, our findings offer valuable insights into the growing body of evidence that supports a role for a combination of innate immune activation, hematopoietic dysregulation, T cell exhaustion, and chronic inflammation in the pathogenesis of LC with ME/CFS.

Thus, this study contributes to a comprehensive knowledge base for a better understanding of LC pathophysiology and may have potential future therapeutic implications.

Nevertheless, our study was limited by a single-point sample collection. Hence, there is a need for future large-scale multi-centered studies across various LC subgroups, including those with and without ME/CFS. Additionally, our study focused on COVID-19 patients infected with the Wuhan strain and Delta/Omicron variants. Given the varying effects of SARS-CoV-2 variants on the immune system [87,88], further studies in LC individuals infected with different variants of concerns are warranted.

Declaration of competing interest

The authors declare no competing interests.

Data availability

Data will be made available on request.

Acknowledgments

We thank our study volunteers for providing samples and supporting this work and the clinical staff for their dedication to this research, in particular, Dr. Maeve Smith the Co-director of the LC clinic.

This work was primarily supported by a grant from the Canadian Institutes of Health Research (CIHR # 174901), and another grant from Li Ka Shing Institute Virology (both to SE). MO is supported by the Arthritis Society through a STAR/IMHA award (award 00049). DR and JWCT are supported by the Dutch Kidney Foundation. We also acknowledge the LC Facebook community of Alberta for their contribution to this study. Biorender.com enabled us to make the graphic summary.

Appendix A. Supplementary data

Supplementary data to this article can be found online at https://doi.org/10.1016/j.jaut.2024.103267. I was unable to open the supplemental data link. We replaced Supplementary Tables (1 & 2) in the final revison. I just want to make sure that those updated S Tables are incorporated in the manuscript.

References

[1] M. Taquet, Q. Dercon, S. Luciano, J.R. Geddes, M. Husain, P.J. Harrison, Incidence, co-occurrence, and evolution of long-COVID features: a 6-month retrospective cohort study of 273,618 survivors of COVID-19, PLoS Med. 18 (2021) e1003773.
[2] O. f. N. S. (ONS), Prevalence of long COVID symptoms and COVID-19 complications. https://wwwonsgovuk/peoplepopulationandcommunity/healthandsocialcare/healthandlifeexpectancies/datasets/prevalenceoflongcovidsymptomsandcovid19complications, 2020.
[3] A.D. Desai, M. Lavelle, B.C. Boursiquot, E. Wan, Long-term complications of COVID-19, Am. J. Physiol.: Cell Physiol. (2021).
[4] R. Gorna, N. MacDermott, C. Rayner, M. O'Hara, S. Evans, L. Agyen, et al., Long COVID guidelines need to reflect lived experience, Lancet 397 (2021) 455–457.
[5] A. Nath, Long-haul COVID, Neurology 95 (2020) 559–560.
[6] A.V. Ballering, S.K.R. van Zon, T.C. Olde Hartman, J.G.M. Rosmalen, I. Lifelines Corona Research, Persistence of somatic symptoms after COVID-19 in The Netherlands: an observational cohort study, Lancet 400 (2022) 452–461.
[7] C. Phetsouphanh, D.R. Darley, D.B. Wilson, A. Howe, C.M.L. Munier, S.K. Patel, et al., Immunological dysfunction persists for 8 months following initial mild-to-moderate SARS-CoV-2 infection, Nat. Immunol. 23 (2022) 210–216.
[8] J. Muri, V. Cecchinato, A. Cavalli, A.A. Shanbhag, M. Matkovic, M. Biggiogero, et al., Autoantibodies against chemokines post-SARS-CoV-2 infection correlate with disease course, Nat. Immunol. (2023).
[9] M. Haffke, H. Freitag, G. Rudolf, M. Seifert, W. Doehner, N. Scherbakov, et al., Endothelial dysfunction and altered endothelial biomarkers in patients with post-COVID-19 syndrome and chronic fatigue syndrome (ME/CFS), J. Transl. Med. 20 (2022) 138.
[10] Z. Swank, Y. Senussi, Z. Manickas-Hill, X.G. Yu, J.Z. Li, G. Alter, et al., Persistent circulating severe acute respiratory syndrome coronavirus 2 Spike is associated with post-acute coronavirus disease 2019 sequelae, Clin. Infect. Dis. (2022).
[11] M.J. Peluso, S. Lu, A.F. Tang, M.S. Durstenfeld, H.E. Ho, S.A. Goldberg, et al., Markers of immune activation and inflammation in individuals with postacute sequelae of severe acute respiratory syndrome coronavirus 2 infection, J. Infect. Dis. 224 (2021) 1839–1848.
[12] Y. Lopez-Hernandez, J. Monarrez-Espino, D.A.G. Lopez, J. Zheng, J.C. Borrego, C. Torres-Calzada, et al., The plasma metabolome of long COVID patients two years after infection, Sci. Rep. 13 (2023) 12420.
[13] S. Saito, S. Shahbaz, X. Luo, M. Osman, D. Redmond, J.W. Cohen Tervaert, et al., Metabolomic and immune alterations in long COVID patients with chronic fatigue syndrome, Front. Immunol. 15 (2024) 1341843.
[14] N. Bozorgmehr, S. Mashhouri, E. Perez Rosero, L. Xu, S. Shahbaz, W. Sligl, et al., Galectin-9, a player in cytokine release syndrome and a surrogate diagnostic biomarker in SARS-CoV-2 infection, mBio 12 (2021).
[15] L.A. Jason, M. Sunnquist, A. Brown, M. Evans, S.D. Vernon, J. Furst, et al., Examining case definition criteria for chronic fatigue syndrome and myalgic encephalomyelitis, Fatigue 2 (2014) 40–56.
[16] E.J. Lim, Y.C. Ahn, E.S. Jang, S.W. Lee, S.H. Lee, C.G. Son, Systematic review and meta-analysis of the prevalence of chronic fatigue syndrome/myalgic encephalomyelitis (CFS/ME), J. Transl. Med. 18 (2020) 100.
[17] J.W.C. Tervaert, Fatigue in patients with ANCA-associated vasculitis: is avacopan the answer? Lancet Rheumatol. 5 (2023) E429–E430.
[18] C. van Eeden, D. Redmond, N. Mohazab, M.J. Larche, A.L. Mason, J.W. Cohen Tervaert, et al., Evidence of a novel mitochondrial signature in systemic sclerosis patients with chronic fatigue syndrome, Int. J. Mol. Sci. 24 (2023).
[19] H. Bedree, M. Sunnquist, L.A. Jason, The DePaul symptom questionnaire-2: a validation study, Fatigue 7 (2019) 166–179.
[20] M. Maes, F.N.M. Twisk, Why myalgic encephalomyelitis/chronic fatigue syndrome (ME/CFS) may kill you: disorders in the inflammatory and oxidative and nitrosative stress (IO&NS) pathways may explain cardiovascular disorders in ME/CFS, Neuroendocrinol. Lett. 30 (2009) 677–693.
[21] I. Murga Gandasegui, L. Aranburu Laka, P.A. Gargiulo, J.C. Gomez-Esteban, J. V. Lafuente Sanchez, Myalgic encephalomyelitis/chronic fatigue syndrome: a neurological entity? Medicina 57 (2021).
[22] C.M. Galvez-Sanchez, G.A. Reyes Del Paso, Diagnostic criteria for fibromyalgia: critical review and future perspectives, J. Clin. Med. 9 (2020).
[23] F. Wolfe, D.J. Clauw, M.A. Fitzcharles, D.L. Goldenberg, R.S. Katz, P. Mease, et al., The American College of Rheumatology preliminary diagnostic criteria for fibromyalgia and measurement of symptom severity, Arthritis Care Res. 62 (2010) 600–610.
[24] R. Ferrari, A.S. Russell, A questionnaire using the modified 2010 American college of rheumatology criteria for fibromyalgia: specificity and sensitivity in clinical practice, J. Rheumatol. 40 (2013) 1590–1595.
[25] D.E. Broadbent, P.F. Cooper, P. FitzGerald, K.R. Parkes, The cognitive failures questionnaire (CFQ) and its correlates, Br. J. Clin. Psychol. 21 (1982) 1–16.
[26] S. Shahbaz, L. Xu, W. Sligl, M. Osman, N. Bozorgmehr, S. Mashhouri, et al., The quality of SARS-CoV-2-specific T cell functions differs in patients with mild/moderate versus severe disease, and T cells expressing coinhibitory receptors are highly activated, J. Immunol. 207 (2021) 1099–1111.
[27] M. Motamedi, S. Shahbaz, L. Fu, G. Dunsmore, L. Xu, R. Harrington, et al., Galectin-9 expression defines a subpopulation of NK cells with impaired cytotoxic effector molecules but enhanced IFN-gamma production, dichotomous to TIGIT, in HIV-1 infection, Immunohorizons 3 (2019) 531–546.
[28] S. Elahi, J.M. Ertelt, J.M. Kinder, T.T. Jiang, X. Zhang, L. Xin, et al., Immunosuppressive CD71+ erythroid cells compromise neonatal host defence against infection, Nature 504 (2013) 158–162.
[29] S. Elahi, S. Shahbaz, S. Houston, Selective upregulation of CTLA-4 on CD8+ T cells restricted by HLA-B*35Px renders them to an exhausted phenotype in HIV-1 infection, PLoS Pathog. 16 (2020) e1008696.
[30] S. Elahi, W.L. Dinges, N. Lejarcegui, K.J. Laing, A.C. Collier, D.M. Koelle, et al., Protective HIV-specific CD8+ T cells evade Treg cell suppression, Nat. Med. 17 (2011) 989–995.
[31] A. Namdar, G. Dunsmore, S. Shahbaz, P. Koleva, L. Xu, J. Jovel, et al., CD71(+) erythroid cells exacerbate HIV-1 susceptibility, mediate trans-infection, and harbor infective viral particles, mBio 10 (2019).
[32] S. Elahi, M.A. Vega-Lopez, V. Herman-Miguel, C. Ramirez-Estudillo, J. Mancilla-Ramirez, B. Motyka, et al., CD71(+) erythroid cells in human neonates exhibit immunosuppressive properties and compromise immune response against systemic infection in neonatal mice, Front. Immunol. 11 (2020) 597433.
[33] N. Bozorgmehr, I. Okoye, O. Oyegbami, L. Xu, A. Fontaine, N. Cox-Kennett, et al., Expanded antigen-experienced CD160(+)CD8(+)effector T cells exhibit impaired effector functions in chronic lymphocytic leukemia, J. Immunother. Cancer 9 (2021).
[34] S. Elahi, T. Niki, M. Hirashima, H. Horton, Galectin-9 binding to Tim-3 renders activated human CD4+ T cells less susceptible to HIV-1 infection, Blood 119 (2012) 4192–4204.
[35] O.I. Shahbaz S, G. Belvins, S. Elahi, Elevated ATP via enhanced miRNA-30b, 30c, and 30e downregulates the expression of CD73 in CD8+ T cells of HIV-infected individuals, PLoS Pathog. (2022).
[36] L. Li, Z.P. Liu, Biomarker discovery for predicting spontaneous preterm birth from gene expression data by regularized logistic regression, Comput. Struct. Biotechnol. J. 18 (2020) 3434–3446.
[37] M.R. Goeman J, N. Chaturvedi, L1 and L2 Penalized Regression Models, 2022, pp. 9–52.
[38] S. van Buuren, K. Groothuis-Oudshoorn, Mice: multivariate imputation by chained equations in R, J. Stat. Software 45 (2011) 1–67.
[39] J. Friedman, T. Hastie, R. Tibshirani, Regularization paths for generalized linear models via coordinate descent, J. Stat. Software 33 (2010) 1–22.
[40] J.K. Tay, B. Narasimhan, T. Hastie, Elastic net regularization paths for all generalized linear models, J. Stat. Software 106 (2023) 1–31.
[41] S. Saito, N. Bozorgmehr, W. Sligl, M. Osman, S. Elahi, The role of coinhibitory receptors in B cell dysregulation in SARS-CoV-2-infected individuals with severe disease, J. Immunol. (2024).
[42] Y.K. Yeoh, T. Zuo, G.C. Lui, F. Zhang, Q. Liu, A.Y. Li, et al., Gut microbiota composition reflects disease severity and dysfunctional immune responses in patients with COVID-19, Gut 70 (2021) 698–706.
[43] S. Elahi, R.H. Weiss, S. Merani, Atorvastatin restricts HIV replication in CD4+ T cells by upregulation of p21, AIDS 30 (2016) 171–183.
[44] S. Shahbaz, G. Dunsmore, P. Koleva, L. Xu, S. Houston, S. Elahi, Galectin-9 and VISTA expression define terminally exhausted T cells in HIV-1 infection, J. Immunol. (2020).
[45] K. Lee, S. Elahi, S. Mashhouri, C. Ye, Gout presenting as a chronic inflammatory arthritis from immune checkpoint inhibitors: case series, Rheumatology 60 (2021) E441–E443.
[46] L. Liang, Y.M. Zhang, Y.W. Shen, A.P. Song, W.L. Li, L.F. Ye, et al., Aberrantly expressed galectin-9 is involved in the immunopathogenesis of anti-MDA5-positive dermatomyositis-associated interstitial lung disease, Front. Cell Dev. Biol. 9 (2021).
[47] J. Sun, Y. Sui, Y. Wang, L. Song, D. Li, G. Li, et al., Galectin-9 expression correlates with therapeutic effect in rheumatoid arthritis, Sci. Rep. 11 (2021) 5562.
[48] S. Merani, W. Chen, S. Elahi, The bitter side of sweet: the role of Galectin-9 in immunopathogenesis of viral infections, Rev. Med. Virol. 25 (2015) 175–186.

[49] S. Shahbaz, G. Dunsmore, P. Koleva, L. Xu, S. Houston, S. Elahi, Galectin-9 and VISTA expression define terminally exhausted T cells in HIV-1 infection, J. Immunol. 204 (2020) 2474–2491.
[50] H.Y. Chen, Y.F. Wu, F.C. Chou, Y.H. Wu, L.T. Yeh, K.I. Lin, et al., Intracellular galectin-9 enhances proximal TCR signaling and potentiates autoimmune diseases, J. Immunol. 204 (2020) 1158–1172.
[51] I. Okoye, L. Xu, M. Motamedi, P. Parashar, J.W. Walker, S. Elahi, Galectin-9 expression defines exhausted T cells and impaired cytotoxic NK cells in patients with virus-associated solid tumors, J. Immunother. Cancer 8 (2020).
[52] G. Dunsmore, E.P. Rosero, S. Shahbaz, D.M. Santer, J. Jovel, P. Lacy, et al., Neutrophils promote T-cell activation through the regulated release of CD44-bound Galectin-9 from the cell surface during HIV infection, PLoS Biol. 19 (2021) e3001387.
[53] B.S. Rahmati A, S. Elahi, Galectin-9 promotes natural killer cells activity via interaction with CD44, Front. Immunol. 14 (2023).
[54] H.S. Perez, S. Rosero, J. Jovel, C. R O'Neil, L.S. Turvey, P. Parashar, S. Elahi, Differential signature of the microbiome and neutrophils in the oral cavity of HIV-infected individuals, Front. Immunol. (2021).
[55] N. Bozorgmehr, M. Hnatiuk, A.C. Peters, S. Elahi, Depletion of polyfunctional CD26 (high)CD8(+) T cells repertoire in chronic lymphocytic leukemia, Exp. Hematol. Oncol. 12 (2023) 13.
[56] M. Dusseaux, E. Martin, N. Serriari, I. Peguillet, V. Premel, D. Louis, et al., Human MAIT cells are xenobiotic-resistant, tissue-targeted, CD161hi IL-17-secreting T cells, Blood 117 (2011) 1250–1259.
[57] P.K. Sharma, E.B. Wong, R.J. Napier, W.R. Bishai, T. Ndung'u, V.O. Kasprowicz, et al., High expression of CD26 accurately identifies human bacteria-reactive MR1-restricted MAIT cells, Immunology 145 (2015) 443–453.
[58] C. Zhu, A.C. Anderson, A. Schubart, H. Xiong, J. Imitola, S.J. Khoury, et al., The Tim-3 ligand galectin-9 negatively regulates T helper type 1 immunity, Nat. Immunol. 6 (2005) 1245–1252.
[59] S. Shahbaz, L. Xu, M. Osman, W. Sligl, J. Shields, M. Joyce, et al., Erythroid precursors and progenitors suppress adaptive immunity and get invaded by SARS-CoV-2, Stem Cell Rep. 16 (2021) 1165–1181.
[60] H.E. Davis, L. McCorkell, J.M. Vogel, E.J. Topol, Long COVID: major findings, mechanisms and recommendations, Nat. Rev. Microbiol. 21 (2023) 133–146.
[61] S. Elahi, Neglected cells: immunomodulatory roles of CD71(+) erythroid cells, Trends Immunol. 40 (2019) 181–185.
[62] S. Elahi, S. Mashhouri, Immunological consequences of extramedullary erythropoiesis: immunoregulatory functions of CD71(+) erythroid cells, Haematologica 105 (2020) 1478–1483.
[63] S. Elahi, New insight into an old concept: role of immature erythroid cells in immune pathogenesis of neonatal infection, Front. Immunol. 5 (2014) 376.
[64] H. Huerga Encabo, W. Grey, M. Garcia-Albornoz, H. Wood, R. Ulferts, I. V. Aramburu, et al., Human erythroid progenitors are directly infected by SARS-CoV-2: implications for emerging erythropoiesis in severe COVID-19 patients, Stem Cell Rep. 16 (2021) 428–436.
[65] B.H. Foy, J.C.T. Carlson, E. Reinertsen, I.V.R. Padros, R. Pallares Lopez, E. Palanques-Tost, et al., Association of red blood cell distribution width with mortality risk in hospitalized adults with SARS-CoV-2 infection, JAMA Netw. Open 3 (2020) e2022058.
[66] R.H. Baloh, M.G. Tansey, P.A. Lampe, T.J. Fahrner, H. Enomoto, K.S. Simburger, et al., Artemin, a novel member of the GDNF ligand family, supports peripheral and central neurons and signals through the GFR alpha 3-RET receptor complex, Neuron 21 (1998) 1291–1302.
[67] L. Minnema, J. Wheeler, M. Enomoto, S. Pitake, S.K. Mishra, B.D.X. Lascelles, Correlation of artemin and GFRalpha3 with osteoarthritis pain: early evidence from naturally occurring osteoarthritis-associated chronic pain in dogs, Front. Neurosci. 14 (2020) 77.
[68] M. Ilieva, J. Nielsen, I. Korshunova, K. Gotfryd, E. Bock, S. Pankratova, et al., Artemin and an artemin-derived peptide, artefin, induce neuronal survival, and differentiation through ret and NCAM, Front. Mol. Neurosci. 12 (2019).
[69] L.E. Wong, M.E. Gibson, H.M. Arnold, B. Pepinsky, E. Frank, Artemin promotes functional long-distance axonal regeneration to the brainstem after dorsal root crush, Proc. Nat. Acad. Sci. U. S. A. 112 (2015) 6170–6175.
[70] N. Bozorgmehr, I. Okoye, S. Mashhouri, J. Lu, P. Koleva, J. Walker, et al., CD71(+) erythroid cells suppress T-cell effector functions and predict immunotherapy outcomes in patients with virus-associated solid tumors, J. Immunother. Cancer 11 (2023).
[71] Y. Han, Q. Liu, J. Hou, Y. Gu, Y. Zhang, Z. Chen, et al., Tumor-induced generation of splenic erythroblast-like ter-cells promotes tumor progression, Cell 173 (2018) 634–648 e12.
[72] S. Mashhouri, P. Koleva, M. Huynh, I. Okoye, S. Shahbaz, S. Elahi, Sex matters: physiological abundance of immuno-regulatory CD71+ erythroid cells impair immunity in females, Front. Immunol. 12 (2021) 705197.
[73] S. Elahi, Hematopoietic responses to SARS-CoV-2 infection, Cell. Mol. Life Sci. : CMLS 79 (2022) 187.
[74] S. Nencini, M. Ringuet, D.H. Kim, C. Greenhill, J.J. Ivanusic, GDNF, neurturin, and artemin activate and sensitize bone afferent neurons and contribute to inflammatory bone pain, J. Neurosci. 38 (2018) 4899–4911.
[75] M. Rojas, Y. Rodriguez, Y. Acosta-Ampudia, D.M. Monsalve, C.S. Zhu, Q.Z. Li, et al., Autoimmunity is a hallmark of post-COVID syndrome, J. Transl. Med. 20 (2022).
[76] Y. Su, D. Yuan, D.G. Chen, R.H. Ng, K. Wang, J. Choi, et al., Multiple early factors anticipate post-acute COVID-19 sequelae, Cell 185 (2022) 881–895 e20.
[77] J. Klein, J. Wood, J.R. Jaycox, R.M. Dhodapkar, P.W. Lu, J.R. Gehlhausen, et al., Distinguishing features of long COVID identified through immune profiling, Nature (2023).
[78] K. Yin, M.J. Peluso, X. Luo, R. Thomas, M.G. Shin, J. Neidleman, et al., Long COVID manifests with T cell dysregulation, inflammation and an uncoordinated adaptive immune response to SARS-CoV-2, Nat. Immunol. (2024).
[79] M.B. Long, A.J. Howden, H.R. Keir, C.M. Rollings, Y.H. Giam, T. Pembridge, et al., Extensive acute and sustained changes to neutrophil proteomes post-SARS-CoV-2 infection, Eur. Respir. J. (2023).
[80] E. Pasini, G. Corsetti, C. Romano, T.M. Scarabelli, C. Chen-Scarabelli, L. Saravolatz, et al., Serum metabolic profile in patients with long-Covid (PASC) syndrome: clinical implications, Front. Med.-Lausanne 8 (2021).
[81] T. Sonnweber, P. Grubwieser, S. Sahanic, A.K. Böhm, A. Pizzini, A. Luger, et al., The impact of iron dyshomeostasis and anaemia on long-term pulmonary recovery and persisting symptom burden after COVID-19: a prospective observational cohort study, Metabolites 12 (2022).
[82] C. Vollbracht, K. Kraft, Oxidative stress and hyper-inflammation as major drivers of severe COVID-19 and long COVID: implications for the benefit of high-dose intravenous vitamin C, Front. Pharmacol. 13 (2022).
[83] A. Stufano, C. Isgro, L.L. Palese, P. Caretta, L. De Maria, P. Lovreglio, et al., Oxidative damage and post-COVID syndrome: a cross-sectional study in a cohort of Italian workers, Int. J. Mol. Sci. 24 (2023).
[84] L.E. Wong, M.E. Gibson, H.M. Arnold, B. Pepinsky, E. Frank, Artemin promotes functional long-distance axonal regeneration to the brainstem after dorsal root crush, Proc. Nat. Acad. Sci. U. S. A. 112 (2015) 6170–6175.
[85] C. Fernandez-de-las-Penas, J.D. Martin-Guerrero, O.J. Pellicer-Valero, E. Navarro-Pardo, V. Gomez-Mayordomo, M.L. Cuadrado, et al., Female sex is a risk factor associated with long-term post-COVID related-symptoms but not with COVID-19 symptoms: the LONG-COVID-EXP-CM multicenter study, J. Clin. Med. 11 (2022).
[86] S.V. Sylvester, R. Rusu, B. Chan, M. Bellows, C. O'Keefe, S. Nicholson, Sex differences in sequelae from COVID-19 infection and in long COVID syndrome: a review, Curr. Med. Res. Opin. 38 (2022) 1391–1399.
[87] S. Saito, S. Shahbaz, W. Sligl, M. Osman, D.L. Tyrrell, S. Elahi, Differential impact of SARS-CoV-2 isolates, namely, the Wuhan strain, Delta, and Omicron variants on erythropoiesis, Microbiol. Spectr. (2022) e0173022.
[88] S. Shahbaz, N. Bozorgmehr, J. Lu, M. Osman, W. Sligl, D.L. Tyrrell, et al., Analysis of SARS-CoV-2 isolates, namely the Wuhan strain, Delta variant, and Omicron variant, identifies differential immune profiles, Microbiol. Spectr. 11 (2023) e0125623.